SIAM J. APPL. MATH.
Vol. 76, No. 3, pp. 1000–1030

PHASED AND PHASELESS DOMAIN RECONSTRUCTIONS IN THE INVERSE SCATTERING PROBLEM VIA SCATTERING COEFFICIENTS*

HABIB AMMARI†, YAT TIN CHOW‡, AND JUN ZOU§

Abstract. In this work we first review the (phased) inverse scattering problem and then pursue the phaseless reconstruction from far-field data with the help of the concept of scattering coefficients. We perform sensitivity, resolution, and stability analysis of both phased and phaseless problems and compare the degree of ill-posedness of the phased and phaseless reconstructions. The phaseless reconstruction is highly nonlinear and much more severely ill-posed. Algorithms are provided to solve both the phased and the phaseless reconstructions in the linearized case. Stability is studied by estimating the condition number of the inversion process for both the phased and the phaseless cases. An optimal strategy is suggested to attain the infimum of the condition numbers of the phaseless reconstruction, which may provide an important guidance for efficient phaseless measurements in practical applications. To the best of our knowledge, the stability analysis in terms of condition numbers is new for the phased and phaseless inverse scattering problems and is very important to help us understand the degree of ill-posedness of these inverse problems. Numerical experiments are provided to illustrate the theoretical asymptotic behavior, as well as the effectiveness and robustness of the phaseless reconstruction algorithm.

Key words. phaseless reconstruction, inverse medium scattering, scattering coefficients, far-field measurements, condition numbers, reconstruction algorithm

AMS subject classifications. 35R30, 35B30

DOI. 10.1137/15M1043959

1. Introduction.

The inverse scattering problems are well known to be severely ill-posed. It has widespread applications in, e.g., oil/crack detection, target identification, geophysical prospection, nondestructive testing, medical imaging, and physiological measurement [3, 4, 11, 19, 32, 33, 34, 42, 43, 44, 45, 46, 50, 51]. Due to their applications, inverse scattering problems have attracted much attention, and many numerical algorithms have been developed over recent decades for phased reconstruction problems, e.g., time-reversal multiple signal classification methods [24, 38], contrast source inversion methods [2, 3, 4, 44, 45, 46, 47], the continuation method [10], the subspace-based optimization method [15, 16], linear sampling or probing methods [17, 31, 41], the parallel radial bisection method [35], direct sampling methods [22], multilevel sampling methods [30, 36], etc.

However, in many areas of applied sciences it is very difficult and expensive to obtain the phased data of the scattered field, while the phaseless data is much easier to acquire. In addition, the phase of the field is more easily polluted by the noise than the amplitude in many practical situations. For instance, the measurement of the phase

*Received by the editors October 14, 2015; accepted for publication (in revised form) March 18, 2016; published electronically May 26, 2016.

http://www.siam.org/journals/siap/76-3/M104395.html

†Department of Mathematics, ETH Zürich, CH-8092 Zürich, Switzerland (habib.ammari@math.ethz.ch). This author's work was supported by the ERC Advanced Grant Project MULTIMOD–267184.

‡Department of Mathematics, University of California, Los Angeles, CA 90095-1555 (ytchow@math.cuhk.edu.hk). This author's work was partially supported by a Direct Grant for Research from The Chinese University of Hong Kong.

§Department of Mathematics, Chinese University of Hong Kong, Shatin, N.T., Hong Kong (zou@math.cuhk.edu.hk). This author's work was substantially supported by Hong Kong RGC grants (projects 14306814 and 405513).

is extremely difficult when the working frequency is beyond tens of gigahertz, and one cannot expect a good accuracy of the phase measurement [33, 34, 42]. This motivates the phaseless reconstructions and attracts huge attention from both the physics and the mathematics communities. Nonetheless, the phaseless reconstruction is yet much more severely ill-posed than the phased reconstruction; in particular, it appears to be impossible to recover the location of an obstacle only from the modulus of the far-field pattern owing to the fact that it is invariant under translations [29]. In spite of this drastic difficulty, several approaches have been proposed in the literature for the phaseless medium reconstruction in optics, acoustics, and electromagnetics, e.g., the phaseless data multiplicative regularized contrast sources inversion method [32, 52] and several other methods [14, 18, 21, 33, 34, 42, 53]. Also, the phaseless acoustic (sound-soft) obstacle reconstruction was studied in [23], where the reconstruction is split into two parts: the shape reconstruction from the phaseless data and the location of the obstacle from a few phased measurements. Theoretically, the uniqueness of a phaseless scattering reconstruction was established in [25, 26], while the phaseless measurements were connected to the Radon transform of the potential under the Born approximation [28], and a new numerical method was proposed in [27] for the phaseless problem using this connection to the Radon transform. Novikov [39, 40] also introduces reconstruction procedures for the phaseless inverse scattering problems. There are also other works which address both the theoretical and the algorithmic aspects of problems related to phaseless reconstruction of a function or vector, where the phase of a function or vector is recovered from the modulus of its evaluation of a special family of functionals [13, 20, 37], e.g., the coefficients of a Cauchy wavelet transform.

In this work, we study both the phased and the phaseless shape reconstructions from the far-field data of an acoustic medium scattering problem, which is modeled by the following Helmholtz equation:

$$\Delta u + k^2(1 + q(x))\, u = 0 \quad \text{in} \quad \mathbb{R}^2, \tag{1.1}$$

where u is the total field, $q(x) \geq 0$ is the contrast of the medium, and k is the wave number.

Suppose that D is an inclusion contained inside a homogeneous background medium, and it is an open bounded connected domain with a $\mathcal{C}^{1,\alpha}$-boundary for $0 < \alpha < 1$. We consider the contrast q of the form

$$q(x) = \varepsilon^* \chi_D(x), \tag{1.2}$$

where χ_D is the characteristic function of D and $\varepsilon^* > 0$ is a constant. The Helmholtz system (1.1) is often complemented by the physical outgoing Sommerfeld radiation condition:

$$\left| \frac{\partial}{\partial |x|} u^s - iku^s \right| = O(|x|^{-\frac{3}{2}}) \quad \text{as} \quad |x| \to \infty\,, \tag{1.3}$$

where $u^s := u - u^i$ is the scattered field and u^i is the incident wave. Now we can see that the solution u to the system (1.1)–(1.3) represents the total field due to the scattering from the inclusion D corresponding to the incident u^i. Then the phased reconstruction is to recover the shape of D from the phased measurements of either the scattered field or the far-field, while the phaseless reconstruction is to recover the shape of D from only the magnitude of the scattered field or the far-field.

We shall analyze the sensitivity, resolution, and stability of both the phased and the phaseless reconstructions in the linearized cases under certain measurement strategies and compare the major differences between these two reconstructions. With the help of these analyses, we will propose an efficient measurement method which leads to a well-posed inversion process of the phaseless reconstruction. As demonstrated by our early works [6, 8, 9], the scattering coefficients provide a powerful and efficient tool for shape classification of a target domain, and this concept will also persist in this work to help us establish stable reconstruction algorithms and their analysis.

We start by recalling the phased reconstruction in the linearized case so as to provide important insight into the highly nonlinear phaseless reconstruction problems. Within this framework, we shall provide a resolution analysis on numerical reconstruction with phased data in terms of signal-to-noise ratio and then propose algorithms for shape reconstructions with the phased measurement. Another major focus of this work is the stability of the phaseless reconstruction, for which we will provide an efficient algorithm and estimate the condition number of the phaseless inversion process. We are able to establish a sharp upper bound for the infimum of the condition numbers of the inversion process over all phaseless measurement strategies for a given target resolution and hence propose an optimal modulus measurement method. A similar analysis is carried out for the phased reconstruction to allow a clear comparison between the phased and phaseless reconstructions. To the best of our knowledge, our stability estimates in terms of condition numbers are completely new to inverse medium scattering problems and appear to be a very important and effective novel tool to help us better understand the degree of ill-posedness and stability of both the phased and the phaseless reconstructions.

The remaining part of the work is organized as follows. In section 2, we review the concept of scattering coefficients and obtain several important results, which will be of crucial importance to connect the scattering coefficients to both the phased and the phaseless reconstructions and to help us develop efficient algorithms and their analysis. Then we move on to the sensitivity analysis of the phased measurement data in section 3, which will also give a link-up between the phaseless data and information about the shape of the domain. An important comparison is provided in section 3 for the similarities and differences between the phased and phaseless reconstructions. A phased reconstruction algorithm in the linearized case is then proposed in section 4, also with a clear resolution analysis of the algorithm. This resolution analysis is very helpful for us to understand the corresponding resolution constraint in the phaseless reconstruction. Next, we introduce our phaseless recovery problem in section 5 and provide a phaseless shape reconstruction algorithm in section 6. A stability analysis is performed for our new phaseless reconstruction algorithm in section 7. Optimal strategies for minimizing the condition number of the inversion process and analysis of the differences between the ill-posed natures of the phased and phaseless reconstructions are also given. Numerical experiments are presented in section 8 to confirm the theoretical estimates of the condition number of our inversion process and illustrate the effectiveness and robustness of our newly proposed phaseless recovery algorithm. We emphasize that, although our analyses are performed only for two dimensions, similar results and analysis can be extended to higher dimensions as well.

2. Revisit to the concept of scattering coefficients and its sensitivity analysis. In this section, we recall the definition of the scattering coefficient [5, 6, 8] and provide some useful results about sensitivity analysis for our subsequent shape

reconstruction. To do so, we first introduce some useful notation [6, 8]. Let Φ_k be the fundamental solution to the Helmholtz equation

$$(\Delta + k^2)\,\Phi_k(x) = \delta_0(x), \tag{2.1}$$

where δ_0 is the Dirac mass at 0, with the outgoing Sommerfeld radiation condition

$$\left|\frac{\partial}{\partial|x|}\Phi_k - ik\Phi_k\right| = O(|x|^{-\frac{3}{2}}) \quad \text{as} \quad |x| \to \infty\,.$$

Then Φ_k can be written in terms of the Hankel function $H_0^{(1)}$ of the first kind of order zero:

$$\Phi_k(x) = -\frac{i}{4}H_0^{(1)}(k|x|)\,. \tag{2.2}$$

Given an incident field u^i satisfying the homogeneous Helmholtz equation

$$\Delta u^i + k^2 u^i = 0\,, \tag{2.3}$$

the solution u to (1.1) and (1.3) can be represented by the Lippmann–Schwinger equation as

$$u(x) = u^i(x) - \varepsilon^* k^2 \int_D \Phi_k(x-y)u(y)dy\,, \quad x \in \mathbb{R}^2\,, \tag{2.4}$$

and the scattered field is given by

$$u^s(x) = -\varepsilon^* k^2 \int_D \Phi_k(x-y)u(y)dy\,, \quad x \in \mathbb{R}^2\,. \tag{2.5}$$

Throughout this work, we shall focus on the plane incident wave u^i of the form $e^{ik\widehat{d}\cdot x}$ with a unit vector $\widehat{d}$.

In what follows, we shall often use the following single-layer potential:

$$S_{\partial D}^k[\phi](x) = \int_{\partial D} \Phi_k(x-y)\phi(y)\,ds(y)\,, \quad \phi \in L^2(\partial D); \tag{2.6}$$

then the scattering coefficients are defined as follows [6, 8].

DEFINITION 2.1. *For $n, m \in \mathbb{Z}$, the scattering coefficients $W_{nm}(D, \varepsilon^*, k)$ are defined by*

$$W_{nm}(D, \varepsilon^*, k) = \int_{\partial\Omega} \mathcal{J}_n(kr_x)\, e^{-in\theta_x}\phi_m(x)\,ds(x)\,, \tag{2.7}$$

where $x = r_x(\cos\theta_x, \sin\theta_x)$ is in polar coordinates, $\mathcal{J}_n$ denotes the Bessel functions of the first kind, and the weight function $\phi_m \in L^2(\partial D)$ is such that the pair $(\phi_m, \psi_m) \in L^2(\partial D) \times L^2(\partial D)$ satisfies the following system of integral equations:

$$\begin{cases} S_{\partial D}^{k\sqrt{\varepsilon^*+1}}[\phi_m](x) - S_{\partial D}^k[\psi_m](x) = \mathcal{J}m(kr_x)e^{im\theta_x}\,, \\ \frac{\partial}{\partial\nu}S_{\partial D}^{k\sqrt{\varepsilon^*+1}}[\phi_m](x)\,|_- - \frac{\partial}{\partial\nu}S_{\partial D}^k[\psi_m](x)\,|_+ = \frac{\partial}{\partial\nu}(\mathcal{J}_m(kr_x)e^{im\theta_x}). \end{cases} \tag{2.8}$$

Here + and − in the subscripts indicate, respectively, the limits from outside D and inside D to ∂D along the normal direction, and $\partial/\partial\nu$ denotes the outward normal derivative.

The scattering coefficients $W_{nm}(D,\varepsilon^*,k)$ are basically the Fourier coefficients of the far-field pattern (a.k.a. the scattering amplitude), which is a 2π-periodic function in two dimensions [5, 6, 8]. For the incident field $e^{ik\widehat{d}\cdot x}$ with a unit vector $\widehat{d}$, we have

$$(u-u^i)(x) = ie^{-\pi i/4}\frac{e^{ik|x|}}{\sqrt{8\pi k|x|}}A_\infty(\widehat{d},\widehat{x},k) + O(|x|^{-\frac{3}{2}}) \quad \text{as } |x|\to\infty,$$

where $\widehat{x} = x/|x| = (\cos\theta_x, \sin\theta_x)$ and $\widehat{d} = (\cos\theta_d, \sin\theta_d)$ are in polar coordinates, and $A(\theta_d,\theta_x,k) := A_\infty(\widehat{d},\widehat{x},k)$ is the so-called far-field pattern. The following results can be found in [5, 6, 8].

THEOREM 2.2. *Let $\mathfrak{F}_{\theta_d,\theta_x}[A(\theta_d,\theta_x,k)](m,n)$ be the (m,n)th Fourier coefficient of the far-field pattern $A(\theta_d,\theta_x,k)$ of a general domain D with the background wavenumber k; then it holds that*

$$W_{nm}(D,\varepsilon^*,k) = i^{(n-m)}\mathfrak{F}_{\theta_d,\theta_x}[A(\theta_d,\theta_x,k)](-m,n), \tag{2.9}$$

or equivalently,

$$A(\theta_d,\theta_x,k) = \sum_{m,n\in\mathbb{Z}} i^{(m-n)}e^{-im\theta_d}e^{in\theta_x}W_{nm}(D,\varepsilon^*,k)\,. \tag{2.10}$$

The following result is a direct consequence of Corollary 7.1 in [6].

THEOREM 2.3. *When the contrast ε^* is small, it holds, for a general domain D, that*

$$W_{nm}(D,\varepsilon^*,k) = \varepsilon^* k^2\int_D \mathcal{J}_n(kr)\mathcal{J}_m(kr)e^{i(n-m)\theta}\,dx + O(\varepsilon^{*2})\,. \tag{2.11}$$

The expression can be simplified in the special case when the domain is a circular shape $B := B_R(0)$ as

$$W_{nm}(B,\varepsilon^*,k) = 2\pi\varepsilon^*\delta_{nm}k^2\int_0^R [\mathcal{J}_n(kr)]^2 r\,dr + O(\varepsilon^{*2}), \tag{2.12}$$

where δ_{nm} is the Kronecker delta.

We remark that the integral appearing in (2.12) can be calculated explicitly as a Lommel integral, and this fact will become very helpful in section 3.

Before going to the discussion about the phased and phaseless reconstructions, we shall first provide a sensitivity estimate of the scattering coefficient under a perturbation of an open ball B, which is important for our subsequent analysis about the resolution of both the phased and the phaseless reconstructions. Our sensitivity analysis is performed by examining the variational derivative along a direction $h\in C^1(\partial B)$ on ∂B, and we refer to this as a linearization process.

Now, let $\nu(x)$ be the outward unit normal to ∂B, and let $D := B^\delta$ be a δ-perturbation of B along the variational direction $h\in C^1(\partial B)$ with $||h|| = 1$:

$$\partial B^\delta := \{\tilde{x} = x + \delta h(x)\nu(x) \,:\, x\in\partial B\}\,; \tag{2.13}$$

then we can write the difference between the integrals over the domains B and B^δ for an L^1 function f:

$$\int_{B^\delta} f(x)dx - \int_B f(x)dx = \delta \int_{\partial B} f(x)h(x)\, ds(x) + O(\delta^2)\,.$$

Now it follows from this and (2.11) that

$$\begin{aligned}
&W_{nm}(B^\delta, \varepsilon^*, k) - W_{nm}(B, \varepsilon^*, k)\\
&= \varepsilon^* k^2 \int_{B^\delta \bigcup B\setminus B^\delta \bigcap B} \operatorname{sgn}(h)\mathcal{J}_n(kr)\mathcal{J}_m(kr)e^{i(n-m)\theta}\, dx + O\left(\varepsilon^*\delta^2 + \varepsilon^{*2}\right)\\
&= \varepsilon^*\delta k^2 \int_{\partial B} h(x)\mathcal{J}_n(kr)\mathcal{J}_m(kr)e^{i(n-m)\theta}\, dx + O\left(\varepsilon^*\delta^2 + \varepsilon^{*2}\right)\\
&= \varepsilon^* R\delta k^2 \mathcal{J}_n(kR)\mathcal{J}_m(kR)\int_0^{2\pi} h(\theta)e^{i(n-m)\theta}\, d\theta + O\left(\varepsilon^*\delta^2 + \varepsilon^{*2}\right)\\
&= 2\pi R k^2 \varepsilon^*\delta \mathcal{J}_n(kR)\mathcal{J}_m(kR)\mathfrak{F}[h](n-m) + +O\left(\varepsilon^*\delta^2 + \varepsilon^{*2}\right)\,,
\end{aligned}$$

where $\mathfrak{F}[h](n-m)$ stands for the $(n-m)$th Fourier coefficient of the perturbation h in the argument θ.

If we further require that the magnitude of δ is larger than ε^* in a way such that $\delta = (\varepsilon^*)^\alpha$ for some $0 < \alpha < 1$, then we arrive at the following result by some argument similar to that in [5].

THEOREM 2.4. *Let $D := B^\delta$ be a δ-perturbation of $B := B_R(0)$ as defined in* (2.13)*; then it holds for $\delta = (\varepsilon^*)^\alpha$ with $0 < \alpha < 1$ that*

$$\begin{aligned}
&W_{nm}(B^\delta, \varepsilon^*, k) - W_{nm}(B, \varepsilon^*, k)\\
&= 2\pi R k^2 (\varepsilon^*)^{1+\alpha}\mathcal{J}_n(kR)\mathcal{J}_m(kR)\mathfrak{F}[h](n-m) + O(\varepsilon^*)^2.
\end{aligned} \tag{2.14}$$

3. Sensitivity analysis of the phased measurement data. In this section, we shall develop a sensitivity analysis of the phased measurement of the far-field data based on the result for the scattering coefficients in Theorem 2.4. This shall help us provide a crucial expression between the phaseless measurement of the far-field data (i.e., only its magnitude) and the shape D.

Suppose that $D := B^\delta$ is a δ-perturbation of $B := B_R(0)$ along the variational direction $h \in C^1(\partial D)$ with $||h|| = 1$ as described earlier. Then it follows from (2.10), (2.12), and (2.14) that

$$\begin{aligned}
&A_\infty(\theta, \widetilde{\theta}, k)\\
&= \sum_{n,m\in\mathbb{Z}} i^{n-m}e^{in\theta}e^{-im\widetilde{\theta}}\, W_{nm}(B^\delta, \varepsilon^*, k)\\
&= 2\pi\varepsilon^* k^2 \sum_{l\in\mathbb{Z}} e^{il(\theta-\widetilde{\theta})}\int_0^R [\mathcal{J}_l(kr)]^2 r dr\\
&\quad + 2\pi R\,(\varepsilon^*)^{1+\alpha}k^2 \sum_{n,l\in\mathbb{Z}} i^l e^{il\widetilde{\theta}}e^{in(\theta-\widetilde{\theta})}\mathcal{J}_n(kR)\mathcal{J}_{n-l}(kR)\mathfrak{F}[h](l) + O(\varepsilon^*)^2\,.
\end{aligned}$$

Although the above expression looks quite complicated, it can be greatly simplified by some well-known properties of the Bessel functions. In fact, using the following

form of Graf's addition formula [48],

$$\begin{aligned}&\sum_{n=-\infty}^{\infty} \mathcal{J}_n(x)\mathcal{J}_{n-l}(y)e^{in\theta}\\ &= (-1)^l \left(\frac{x-y\exp(-i\theta)}{x-y\exp(i\theta)}\right)^{l/2} \mathcal{J}_l\left(\sqrt{x^2+y^2-2xy\cos(\theta)}\right)\end{aligned} \tag{3.1}$$

for $x, y > 0$ and $x \neq y$, and the well-known property for the second Lommel integral,

$$\int_0^R [\mathcal{J}_l(kr)]^2 r dr = \frac{R^2}{2}[\mathcal{J}_l(kR)^2 - \mathcal{J}_{l-1}(kR)\mathcal{J}_{l+1}(kR)]\,, \tag{3.2}$$

we can significantly simplify the above expression of the far-field pattern as

$$\begin{aligned}A_\infty(\theta,\widetilde{\theta},k) &= \pi R^2 \varepsilon^* k^2 \sum_{l\in\mathbb{Z}} e^{il(\theta-\widetilde{\theta})}[\mathcal{J}_l(kR)^2 - \mathcal{J}_{l-1}(kR)\mathcal{J}_{l+1}(kR)]\\ &\quad + 2\pi R\,(\varepsilon^*)^{1+\alpha}\, k^2 \sum_{n,l\in\mathbb{Z}} i^l e^{il\widetilde{\theta}} e^{in(\theta-\widetilde{\theta})} \mathcal{J}_n(kR)\mathcal{J}_{n-l}(kR)\mathfrak{F}[h](l) + O(\varepsilon^*)^2\\ &= \pi R^2 \varepsilon^* k^2 [\mathcal{J}_0(2kR\sin((\widetilde{\theta}-\theta)/2)) - \mathcal{J}_2(2kR\sin((\widetilde{\theta}-\theta)/2))]\\ &\quad + 2\pi R\,(\varepsilon^*)^{1+\alpha} k^2 \sum_{l\in\mathbb{Z}} (-i)^l e^{il(\widetilde{\theta}+\theta)/2} \mathcal{J}_l(2kR\sin((\widetilde{\theta}-\theta)/2))\mathfrak{F}[h](l) + O(\varepsilon^*)^2\,.\end{aligned} \tag{3.3}$$

An interesting point to note is that the constants πR^2 and $2\pi R$ in front of the two terms ε^* and $(\varepsilon^*)^{1+\alpha}$ are, respectively, the volume and surface area of the open ball of radius R.

Summarizing the above discussions, we come directly to the following theorem.

THEOREM 3.1. *If $\delta = (\varepsilon^*)^\alpha$ for $0 < \alpha < 1$, then*

$$\begin{aligned}&A_\infty(\theta,\widetilde{\theta},k)\\ &= \pi R^2 \varepsilon^* k^2 P_R(\theta,\widetilde{\theta},k) + 2\pi R\,(\varepsilon^*)^{1+\alpha} k^2 \langle \mathfrak{F}[h], S_R(\theta,\widetilde{\theta},k)\rangle_{l^2(\mathbb{C})} + O(\varepsilon^*)^2,\end{aligned} \tag{3.4}$$

where $P_R(\theta,\widetilde{\theta},k)$ represents the quantity

$$P_R(\theta,\widetilde{\theta},k) := \mathcal{J}_0(2kR\sin((\widetilde{\theta}-\theta)/2)) - \mathcal{J}_2(2kR\sin((\widetilde{\theta}-\theta)/2)) \tag{3.5}$$

and $S_R(\theta,\widetilde{\theta},k) \in l^2(\mathbb{C})$ is a vector given by

$$S_R(\theta,\widetilde{\theta},k)_l := i^l e^{-il(\widetilde{\theta}+\theta)/2} \mathcal{J}_l(2kR\sin((\widetilde{\theta}-\theta)/2))\,. \tag{3.6}$$

With the above estimate of the far-field pattern, we can calculate the expression of the magnitude of the far-field pattern, namely $|A_\infty(\theta,\widetilde{\theta},k)|$, by

$$\begin{aligned}\frac{|A_\infty(\theta,\widetilde{\theta},k)|^2 - \pi^2 R^4 (\varepsilon^*)^2 k^4 \left(P_R(\theta,\widetilde{\theta},k)\right)^2}{4\pi^2 R^3 (\varepsilon^*)^{2+\alpha} k^4 P_R(\theta,\widetilde{\theta},k)} &= \mathrm{Re}\langle \mathfrak{F}[h], S_R(\theta_i,\widetilde{\theta},k)\rangle_{l^2(\mathbb{C})} + O(\varepsilon^*)^{1-\alpha}\\ &= \langle \mathfrak{F}[h], S_R(\theta,\widetilde{\theta},k)\rangle_{l^2(\mathbb{R}^2)} + O(\varepsilon^*)^{1-\alpha}\,.\end{aligned} \tag{3.7}$$

Due to its great importance for the subsequent phased and phaseless reconstructions, we state it in the following corollary.

COROLLARY 3.2. *For $\delta = (\varepsilon^*)^\alpha$, for $0 < \alpha < 1$ it holds that*

$$\begin{aligned}&\langle \mathfrak{F}[h], S_R(\theta, \widetilde{\theta}, k)\rangle_{l^2(\mathbb{R}^2)}\\ &= \frac{|A_\infty(\theta,\widetilde{\theta},k)|^2 - \pi^2 R^4 (\varepsilon^*)^2 k^4 \left(P_R(\theta,\widetilde{\theta},k)\right)^2}{4\pi^2 R^3 (\varepsilon^*)^{2+\alpha} k^4 P_R(\theta,\widetilde{\theta},k)} + O(\varepsilon^*)^{1-\alpha}\,.\end{aligned} \tag{3.8}$$

One interesting observation is that $P_R(\theta, \widetilde{\theta}, k)$ and $S_R(\theta, \widetilde{\theta}, k)$ become very simple for $\theta = \widetilde{\theta}$:

$$P_R(\theta, \theta, k) = 1\,, \quad S_R(\theta, \widetilde{\theta}, k)_l = \delta_{l0}\,. \tag{3.9}$$

And the expression for the far-field pattern is simplified to

$$A_\infty(\theta, \theta, k) = \pi R^2 \varepsilon^* k^2 + 2\pi R\,(\varepsilon^*)^{1+\alpha} k^2 \mathfrak{F}[h](0) + O(\varepsilon^*)^2, \tag{3.10}$$

which illustrates that the direct backscattering data $A_\infty(\theta, \theta, k)$ may only provide the information about the area and volume of the inclusions but not the first order perturbation.

We end this section with an important remark about some similarities and differences between the phased and phaseless reconstructions in the linearized case. We see from (3.4) that

$$\langle \mathfrak{F}[h], S_R(\theta, \widetilde{\theta}, k)\rangle_{l^2(\mathbb{C})} = \frac{A_\infty(\theta,\widetilde{\theta},k) - \pi R^2 \varepsilon^* k^2 P_R(\theta,\widetilde{\theta},k)}{2\pi R^2 (\varepsilon^*)^{1+\alpha} k^2} + O(\varepsilon^*)^{1-\alpha}\,, \tag{3.11}$$

which might be comparable to Corollary 3.2 above. However, we do see several differences here. First, we obtain an approximate value of $\langle \mathfrak{F}[h], S_R(\theta, \widetilde{\theta}, k)\rangle_{l^2(\mathbb{C})}$ with the phased measurements in the linearized case, while we obtain an approximate value of $\langle \mathfrak{F}[h], S_R(\theta, \widetilde{\theta}, k)\rangle_{l^2(\mathbb{R}^2)}$ with the phaseless measurements, which is the projection of the original complex inner product to the real part. Therefore, we can regard the linearized phaseless reconstruction as a "half-dimension" analogy of the linearized phased reconstruction. Second, in the phased reconstruction, the denominator of the right-hand side of (3.11) does not involve the division of the term $P_R(\theta, \widetilde{\theta}, k)$, whereas in the phaseless reconstruction the division of the term is involved (cf. (3.8)). Both differences make the phaseless reconstruction more ill-posed than the phased one. These differences will be clearly elaborated in section 7.3. As the last point, it is well known that the phaseless reconstruction is not unique in the sense that any translation of the inclusion yields the same phaseless measurement. But this is not reflected from the above equation, as we have assumed the inclusion is in the center for the sake of exposition.

4. A phased reconstruction algorithm in the linearized case. In this section, we provide a reconstruction algorithm for the phased measurement in the linearized case using the concept of the scattering coefficients and then a resolution analysis of this algorithm.

4.1. An algorithm for phased reconstruction. We recall that ε^* is the contrast of the inclusion D (cf. (1.2)) and the perturbation parameter δ of D is of the order $\delta = (\varepsilon^*)^\alpha$ for $0 < \alpha < 1$. Then, motivated by the results in Theorems 2.2 and 2.4, we come to the following reconstruction algorithm in the linearized case.

Algorithm 1. Given the measurement $A_\infty^{\text{meas}}(\theta, \widetilde{\theta}, k)$.

1. Compute W_{nm}^{meas} from the Fourier transform as in (2.9) for $-N < n, m < N$.
2. Find R, ε^* from the following minimization problem:

$$\min_{R,\,\varepsilon^*} \sum_{-N<n<N} \left| W_{nn}^{\text{meas}} - \pi R^2 \varepsilon^* k^2 [\mathcal{J}_l(kR)^2 - \mathcal{J}_{l-1}(kR)\mathcal{J}_{l+1}(kR)] \right|^2 . \tag{4.1}$$

3. Compute from (2.14) the estimator $(\delta\,\mathfrak{F}[h])^{est}$ of the product of magnitude δ and Fourier coefficients $\mathfrak{F}[h]$ of the perturbation h for $l \neq 0$:

$$(\delta\,\mathfrak{F}[h])^{est} := \frac{1}{2N-l} \sum_{m-n=l,\,-N<n,m<N} \frac{W_{nm}^{\text{meas}} - W_{nm}(B, \varepsilon^*, k)}{2\pi R \varepsilon^* k^2 \mathcal{J}_n(kR)\mathcal{J}_m(kR)} . \tag{4.2}$$

Two remarks are in order. First, regarding the nonlinear squared minimization (4.1), a direct application of the descent-type/Newton-type algorithm may get trapped in local minima. But noting that the terms in the squared nonlinear functions involving R and ε^* have closed forms in terms of Bessel functions, their evaluations are direct. In view of the fact that this is only a two-dimensional optimization problem over (R, ε^*) where R, ε^* are both small, one can perform the optimization by a direct exhaustion of the values (R, ε^*) over a grid of small mesh size. The approximate minimizers can be further refined by a descent-type/Newton-type iteration.

Second, we remark that the reconstruction formula (4.2) is similar to the one (5.3) in [5]. Indeed, considering (3.26) in [5] with a contrast ε^*, the Fourier coefficients of any perturbation h of $B = B_R(0)$ can be recovered by an inversion of the operator $A(\varepsilon^*)$ as defined in (4.62) in [5] (after a normalization of its wave number k to $k = 1$). However, the coefficients of the matrix $A(\varepsilon^*)$, i.e., $C(\varepsilon^*, n, m)$ defined in (3.27) in [5], are given only in terms of resolvent operators, and therefore their explicit expressions are not available. The inversion formula (5.3) in [5] is hence inconvenient for a direct usage. Nonetheless, for a small contrast ε^*, we know now from Theorem 2.4 an explicit approximation of coefficients $C(\varepsilon^*, n, m)$ as $C(\varepsilon^*, n, m) \approx 2\pi R k^2 (\varepsilon^*)^{1+\alpha} \mathcal{J}_n(kR)\mathcal{J}_m(kR)$. Therefore, (4.2) can be regarded as an easy-to-use approximation of the inversion formula (5.3) of the operator $A(\varepsilon^*)$ described in [5] when the contrast ε^* is small.

4.2. Resolution analysis with respect to signal-to-noise ratio. In this subsection, we perform a resolution analysis of Algorithm 1 in the previous section, which applies also to other reconstruction process derived from (3.11), since the above algorithm is just a Fourier-transformed version of (3.11). Resolution analysis of the above reconstruction with respect to the signal-to-noise ratio (SNR) can be conducted following the spirit of the work [7].

In what follows, we assume the following noise model for the far-field pattern:

$$A_\infty^{\text{meas}}(\theta_i, \widetilde{\theta}_j, k) := A_\infty(\theta_i, \widetilde{\theta}_j, k) + N(\theta_i, \widetilde{\theta}_j, k), \tag{4.3}$$

where pairs $\{(\theta_i, \widetilde{\theta}_j)\}_{i,j=1}^M$ represent the M incident and receiving angles of the measurement evenly distributed on the circle (where M is very large) and $(N(\theta_i, \widetilde{\theta}_j, k))_{i,j=1}^M$ is modeled as, for any fixed value of k, a complex circular symmetric Gaussian white noise vector with variance:

$$\mathbb{E}[|N(\theta_i, \widetilde{\theta}_j, k)|^2] = \sigma^2 k^4 . \tag{4.4}$$

Here σ represents the noise magnitude and the noise term is assumed to have a variance of quadratic growth with respect to k^4, as it is direct from (2.10) and (2.11)

to see that the magnitude of $A_\infty^{\text{meas}}(\theta_i, \widetilde{\theta}_j, k)$ grows at most in the order of k^2 as k grows.

From the well-known fact that any orthogonal transformation of a Gaussian white random vector will result in another Gaussian white random vector, we arrive at, after taking the discrete Fourier transform in the variables θ and $\widetilde{\theta}$, that the following model for the scattering coefficient should be in force:

$$W_{nm}^{\text{meas}}(B^\delta, \varepsilon^*, k) = W_{nm}(B^\delta, \varepsilon^*, k) + \hat{N}_{n,m,\varepsilon^*}\,, \tag{4.5}$$

where the noise term $\hat{N}_{n,m,\varepsilon^*}$ is another complex circular symmetric Gaussian random variable such that its variance $\mathbb{E}[|\hat{N}_{n,m,\varepsilon^*}|^2]$ (i.e., the power spectrum of the original random variable $N(\theta_i, \widetilde{\theta}_j, k)$) behaves like

$$\mathbb{E}[|\hat{N}_{n,m,\varepsilon^*}|^2] = \sigma^2 k^4\,. \tag{4.6}$$

Assume a generic pair (k, R) such that $k > 1$, $R < 1$, and kR is not a zero of $\mathcal{J}_n$ for all n. Then, for $l \neq 0$, we obtain from a direct subtraction of (2.14) from (4.2), together with (4.5), that

$$\mathfrak{F}[h](l) = (\mathfrak{F}[h])^{est}(l) + \frac{\sigma}{(\varepsilon^*)^{1+\alpha}} N_l + (\varepsilon^*)^{1-\alpha} V_l\,,$$

where V_l represents a deterministic approximation error that is of order 1 with respect to ϵ such that $(\varepsilon^*)^2 V_l$ constitutes the approximation error term of order $O(\varepsilon^*)^2$ in (2.14), and N_l stands for a random noise term satisfying the following estimate for its variance with a small $R < 1$ and large $N < M$ by using (4.6):

$$\begin{aligned}
\mathbb{E}[|N_l|^2] &= \frac{k^4}{4\pi^2(2N-l)^2} \sum_{m-n=l,\ -N<n,m<N} k^{-4} R^{-2} [\mathcal{J}_n(kR)\mathcal{J}_m(kR)]^{-2} \\
&\leq \frac{C_0^2}{(2N-l)^2} \sum_{m-n=l,\ -N<n,m<N} \frac{m^{2m+1} n^{2n+1}}{k^{2(m+n)} R^{2(m+n)+2}} \\
&\leq C_0^2 \frac{N^{4N}}{R^{2+4N}}\,,
\end{aligned} \tag{4.7}$$

where the first inequality comes from the following asymptotic behavior of the Bessel function [1]:

$$\mathcal{J}_n(t) \Big/ \frac{1}{\sqrt{2\pi|n|}} \left(\frac{et}{2|n|}\right)^{|n|} \to 1 \tag{4.8}$$

as $|n| \to \infty$, and constant C_0 is an appropriate constant from this asymptotic estimate. Assuming further that $\varepsilon^* \ll \sqrt{\sigma}$ and

$$\text{SNR} := \left(\frac{\varepsilon^*}{\sigma}\right)^2\,,$$

we get

$$\begin{aligned}
&\mathbb{E}[(\mathfrak{F}[h])^{est}(l)] = \mathfrak{F}[h](l) + O(\varepsilon^*)^{1-\alpha}, \\
&\mathbb{E}\left[\left|(\mathfrak{F}[h])^{est}(l) - \mathbb{E}[(\mathfrak{F}[h])^{est}(l)]\right|^2\right] \leq C_0^2 \frac{N^{4N}}{R^{2+4N}} (\text{SNR})^{-(1+\alpha/2)}\,,
\end{aligned} \tag{4.9}$$

which enables us to conclude the following result.

THEOREM 4.1. *Suppose that $k > 1$, $R < 1$, $\delta = (\varepsilon^*)^\alpha$ for $0 < \alpha < 1$ and $0 < \varepsilon^* \ll 1$, and the number of measurement points $M \gg 1$. If $N < M$ is selected such that*

$$C_0^2 \frac{N^{4N}}{R^{2+4N}} < (\mathrm{SNR})^{1+\alpha/2} \tag{4.10}$$

and that $\mathfrak{F}[h](l)$ ($|l| \leq N$) are of order 1, then the lth mode of h can be resolved for $|l| \leq N$ with an error of $O(\varepsilon^*)^{1-\alpha}$, i.e.,

$$\begin{aligned} &\mathbb{E}[(\mathfrak{F}[h])^{est}(l)] = \mathfrak{F}[h](l) + O(\varepsilon^*)^{1-\alpha}, \\ &\mathbb{E}\left[\left|(\mathfrak{F}[h])^{est}(l) - \mathbb{E}[(\mathfrak{F}[h])^{est}(l)]\right|^2\right] \leq 1\,. \end{aligned} \tag{4.11}$$

5. Introduction to phaseless reconstruction. Phaseless reconstruction originates from the physical background that we can usually only measure the magnitude of some data, for example, the magnitude of the far-field pattern. As briefly explained in section 1, it is quite difficult and expensive to obtain the phased data in many physical and engineering applications, and the phase of a measurement is easily contaminated by noise. On the other hand, the phaseless data is much easier to obtain and less contaminated in many practical situations. Due to these facts, the phaseless reconstruction has attracted wide attention.

5.1. Brief history of a general phaseless reconstruction problem. Let us first give a brief introduction and history of a general phaseless reconstruction. As in [12], for a given set of m sampling vectors, $\mathbf{z}_1, \ldots, \mathbf{z}_m$, we intend to recover a vector $\mathbf{x}$ from some phaseless data. This may be formulated as follows:

$$\text{Find } \mathbf{x} \text{ such that } A(\mathbf{x}) = b, \tag{5.1}$$

where $A : \mathbb{C}^N \to R^m$ is given by $A(\mathbf{x})_i = |\langle \mathbf{x}, \mathbf{z}_i \rangle|^2$. One may consider a convexification of the problem (5.1) [12]:

$$\text{Find } \mathbf{X} \geq 0 \text{ such that } \mathcal{A}(\mathbf{X}) = b\,, \tag{5.2}$$

where $\mathcal{A} : \mathcal{H}^{N\times N} \to R^m$ is given by $\mathcal{A}(\mathbf{X}) = \mathbf{z}_i^* \mathbf{X} \mathbf{z}_i$, which helps reduce the complexity of solving the problem, as well as provides uniqueness results under some practical conditions. For instance, this problem is proven to have a high probability such that it is uniquely solvable up to a unit complex number stably from $O(N \log N)$ random measurements [20]. We remark that a stabilized version of convexification is given by the following:

$$\text{Find } \mathbf{X} \geq 0 \text{ such that } ||\mathcal{A}(\mathbf{X}) - b|| \leq \epsilon ||X_0||_2\,. \tag{5.3}$$

Another more general form of phaseless reconstruction (which generalizes the above) comes from recovering the phase of a function/vector from the modulus of its evaluation by a family of functionals. In a more precise way, let E be a complex vector space and $\{L_i\}_{i\in I}$ be a family of functionals. Then this phaseless reconstruction reads as follows:

$$\text{Find } \mathbf{f} \in E \text{ such that } |L_i(\mathbf{f})| = b\,. \tag{5.4}$$

In the case where $\{L_i\}_{i\in I}$ represents the wavelet transform by the Cauchy wavelets, it was shown in [37] that the modulus of the wavelet transform uniquely determines the function up to a global phase, and the reconstruction operator is continuous but not uniformly continuous.

5.2. Introduction to our phaseless reconstruction problem. The convexification discussed in section 5.1 is a very interesting approach, but the purpose, framework, and analysis of our phaseless reconstruction here are very different. We aim to achieve numerical reconstructions of inhomogeneous domains in the linearized case. We will provide an algorithm for the domain reconstruction from some phaseless far-field data, estimate the condition number of this reconstruction process, and establish an upper bound of its infimum over all phaseless measurement strategies. This casts light on how we can obtain an optimal strategy to perform effective phaseless measurements such that the phaseless inversion process shall be well-posed. For comparison purposes, a similar analysis technique is also performed on its phased counterpart, and a comparison between the phased and phaseless reconstructions shall be made.

6. Phaseless domain reconstruction algorithm in linearized cases. In this section, we provide a new method for the domain reconstruction from the phaseless far-field data based on our analyses and results in sections 2 and 3. We consider a finite number of M measurements of $|A(\theta,\widetilde{\theta},k)|$ at some specific incidence and measurement angles as well as frequencies $\{(\theta_i,\widetilde{\theta}_i,k_i)\}_{i=1}^M$. We would like to remark that the notation $(\theta_i,\widetilde{\theta}_i,k_i)$ is used only to allow a larger degree of freedom in choosing the incidence/measurement angles and the wave-number, not indicating any dependence among the incidence angles, measurement angles, and wave-numbers.

We first recall from Corollary 3.2 the relation

$$\begin{aligned}&\frac{|A_\infty(\theta_i,\widetilde{\theta}_i,k_i)|^2-\pi^2R^4(\varepsilon^*)^2k^4\left(P_R(\theta_i,\widetilde{\theta}_i,k_i)\right)^2}{4\pi^2R^3(\varepsilon^*)^{2+\alpha}k^4P_R(\theta_i,\widetilde{\theta}_i,k_i)}\\ &=\langle\mathfrak{F}[h],S_R(\theta_i,\widetilde{\theta}_i,k_i)\rangle_{l^2(\mathbb{R}^2)}+O(\varepsilon^*)^{1-\alpha}\,,\end{aligned}\tag{6.1}$$

where $P_R(\theta_i,\widetilde{\theta}_i,k_i)\in\mathbb{R}$ and $S_R(\theta_i,\widetilde{\theta}_i,k_i)\in l^2(\mathbb{C})$ are given in (3.5) and (3.6). Therefore, from a finite number of M measurements $|A_\infty(\theta_i,\widetilde{\theta}_i,k_i)|$ $(1\le i\le M)$, we obtain the following linear approximation of $\langle\mathfrak{F}[h],S_R(\theta_i,\widetilde{\theta}_i,k_i)\rangle$ as the measurement quantities from the phaseless measurements:

$$\langle\mathfrak{F}[h],S_R(\theta_i,\widetilde{\theta}_i,k_i)\rangle_{l^2(\mathbb{R}^2)}\approx\frac{|A_\infty(\theta_i,\widetilde{\theta}_i,k_i)|^2-\pi^2R^4(\varepsilon^*)^2k^4|P_R(\theta_i,\widetilde{\theta}_i,k_i)|^2}{4\pi^2R^3(\varepsilon^*)^{2+\alpha}k^4P_R(\theta_i,\widetilde{\theta}_i,k_i)}\,.\tag{6.2}$$

This is of crucial importance for us to derive an algorithm for the domain reconstruction from the phaseless far-field measurements.

6.1. Phaseless reconstruction algorithm. We are now ready to introduce our phaseless reconstruction algorithm. Following Theorem 4.1 from the resolution analysis for the phased reconstruction in section 3, we can directly infer that the resolution with respect to SNR in the phaseless reconstruction should not surpass the Nth Fourier mode, where N satisfies the inequality $C_0^2N^{4N}/R^{2+4N}<(\mathrm{SNR})^{1+\alpha/2}$ for some α, where C_0 is the constant as in Theorem 4.1. Hence in our reconstruction algorithm, we may always assume that $\mathfrak{F}[h](l)=0$ for $|l|>N$ for some N and consider only the inversion of finite-dimensional operators, and the contribution of $\mathfrak{F}[h](l)$ for $|l|>N$ to the measurement data can be regarded as noise. Now since $h(\theta)\in\mathbb{R}$ for all θ, we have the following additional constraints on the Fourier coefficients:

$$\mathfrak{F}[h](-l)=\overline{\mathfrak{F}[h](l)}\,.\tag{6.3}$$

This set of constraints is very important in our subsequent analysis. We assume again that the magnitude of the perturbation δ is of the form $\delta = (\varepsilon^*)^\alpha$ for $0 < \alpha < 1$, where ε^* is the contrast of the inclusion. From Corollary 3.2, we can now suggest the following phaseless reconstruction algorithm.

Algorithm 2. Given a positive integer N and M measurements of the magnitude $|A_\infty^{\text{meas}}(\theta_i, \widetilde{\theta}_i, k_i)|$ $(1 \le i \le M)$ of the far-field.

1. Find the pair (R, ε^*) that minimizes the following functional:

$$\sum_{1\le i\le M} \left| |A_\infty^{\text{meas}}(\theta_i, \widetilde{\theta}_i, k_i)|^2 - \pi^2 R^4 k^4 \varepsilon^{*2} \left(P_R(\theta_i, \widetilde{\theta}_i, k_i) \right)^2 \right|^2 , \tag{6.4}$$

   where the values $P_R(\theta_i, \widetilde{\theta}_i, k_i)$ are computed from (3.5).
2. Compute the following quantities for $1 \le i \le M$:

$$\frac{|A_\infty^{\text{meas}}(\theta_i, \widetilde{\theta}_i, k_i)|^2 - \pi^2 R^4 \varepsilon^{*2} k^4 |P_R(\theta_i, \widetilde{\theta}_i, k_i)|^2}{4\pi^2 R^3 \varepsilon^{*2} k^4 P_R(\theta_i, \widetilde{\theta}_i, k_i)} . \tag{6.5}$$

3. Calculate the estimator $(\delta\, \mathfrak{F}[h])^{est}(l)$ of the product of magnitude δ and Fourier coefficient $\mathfrak{F}[h]$ of the perturbation h for $|l| \le N$ by the inversion of the following system of linear equations:

$$\begin{aligned} &\langle (\delta\, \mathfrak{F}[h])^{est}, S_R(\theta_i, \widetilde{\theta}_i, k_i) \rangle_{l^2(\mathbb{R}^2)} \\ &= \frac{|A_\infty^{\text{meas}}(\theta_i, \widetilde{\theta}_i, k_i)|^2 - \pi^2 R^4 \varepsilon^{*2} k^4 |P_R(\theta_i, \widetilde{\theta}_i, k_i)|^2}{4\pi^2 R^3 \varepsilon^{*2} k^4 P_R(\theta_i, \widetilde{\theta}_i, k_i)} \end{aligned} \tag{6.6}$$

   under the constraints

$$(\mathfrak{F}[h])^{est}(-l) = \overline{(\mathfrak{F}[h])^{est}(l)} . \tag{6.7}$$

We remark that the minimization procedure for the function (6.4) can be done similarly as explained in section 4.1 for (4.1). And the algorithm can provide a stable inversion and reasonable resolution of the perturbation h only up to at most the Nth Fourier mode, where N satisfies the inequality $C_0^2 N^{4N}/R^{2+4N} < (\text{SNR})^{1+\alpha/2}$ for some α, with constant C_0 as in Theorem 4.1 of section 4.

7. Stability of the phaseless domain reconstruction. We are now ready to discuss the stability of the phaseless reconstruction by estimating the condition number of this inversion process. Before going into detailed estimates, we shall state our inversion problem in a more concise manner, which will provide a clear framework for our subsequent analysis. For this purpose, we first define three operators for a given pair $(N, M) \in \mathbb{N}$, where two of them are linear in nature while the other one is nonlinear:

1. the componentwise squaring of a vector followed by a subtraction of another known vector, i.e., the action $v_i \mapsto v_i^2 - \pi^2 R^4 \varepsilon^{*2} k^4 |P_R(\theta_i, \widetilde{\theta}_i, k_i)|^2$, which appears in step 2 of Algorithm 2; and we write this nonlinear operator as $F : \mathbb{R}^M \to \mathbb{R}^M$;
2. the componentwise multiplication of a vector $v_i \mapsto 4\pi^2 R^3 \varepsilon^{*2} k^4 P_R(\theta_i, \widetilde{\theta}_i, k_i)\, v_i$, which appears in step 2 of Algorithm 2; and we will write this linear operator as $L : \mathbb{R}^M \to \mathbb{R}^M$;

3. the linear operator $v \mapsto \left(\langle\, v\,, S_R(\theta_i, \widetilde{\theta}_i, k_i)\rangle_{l^2(\mathbb{R}^2)}\right)_{i=1}^{M}$, which appears in Step 3 of Algorithm 2; and we write this linear operator as $T : \mathbb{C}^{2N} \oplus \{0\} \cong \mathbb{R}^{4N} \to \mathbb{R}^M$.

Without loss of generality, we may always choose a radius R such that the zeroth Fourier coefficient $\mathfrak{F}[h](0)$ is zero. With these preparations, we can write (6.6) as

$$(L \circ T)\left[(\delta\, \mathfrak{F}[h])^{est}\right] = F(|A_\infty^{\mathrm{meas}}(\theta_i, \widetilde{\theta}_i, k_i)|)\,. \tag{7.1}$$

Then our phaseless inversion problem can be precisely stated as follows: given a value of SNR, with a number N such that $C_0^2 N^{4N}/R^{2+4N} < (\mathrm{SNR})^{1+\alpha/2}$ for some α, where C_0 is as in Theorem 4.1, we aim to recover the Fourier coefficients $\delta\,(\mathfrak{F}[h]^{est}(l))_{l=-N}^{N} \in \mathbb{C}^{2N} \oplus \{0\} \cong \mathbb{R}^{4N}$ from (7.1) with M measurements:

$$\begin{aligned}(b_i)_{i=1}^M &:= F(|A_\infty^{\mathrm{meas}}(\theta_i, \widetilde{\theta}_i, k_i)|)\\ &= \left(|A_\infty^{\mathrm{meas}}(\theta_i, \widetilde{\theta}_i, k_i)|^2 - \pi^2 R^4 \varepsilon^{*2} k^4 |P_R(\theta_i, \widetilde{\theta}_i, k_i)|^2\right)_{i=1}^{M} \in \mathbb{R}^M\end{aligned}$$

subjected to the following extra set of constraints in $\mathbb{R}^{4N}$ as

$$\mathrm{Re}(\mathfrak{F}[h])^{est}(-l) - \mathrm{Re}(\mathfrak{F}[h])^{est}(l) = 0\,, \qquad \mathrm{Im}(\mathfrak{F}[h])^{est}(-l) + \mathrm{Im}(\mathfrak{F}[h])^{est}(l) = 0\,.$$

From now on, we denote this set of linear constraints as

$$C\left[(\delta\, \mathfrak{F}[h])^{est}\right] = 0\,. \tag{7.2}$$

After this restatement of the phaseless reconstruction problem, we can directly infer that the stability of the inversion lies in the stability of inversion of the linear operators L and T in the subspace $\ker(C)$ under a certain noise level. Therefore, the aim of this section is to estimate the condition numbers of the operators T and L in this subspace. To the best of our knowledge, the stability estimates on condition numbers are novel for inverse problems, and are very important for us to understand the degree of ill-posedness and stability of the reconstruction problem, as well as to provide optimal methods to minimize these two condition numbers by making wise measurements or regularizations.

7.1. Estimation of the condition number of operator T. We now come to the estimate of the condition number of operator T. For notational sake, we first introduce two more operators, $\iota_0 : \mathbb{C} \to \mathbb{R}^2\,,\ z \mapsto (\mathrm{Re}(z), \mathrm{Im}(z))$, and their liftings on the linear operators over the corresponding spaces

$$\iota : \mathfrak{L}(\mathbb{C}) \cong \mathbb{C} \to \mathfrak{L}(\mathbb{R}^2) \cong M_{2\times 2}\,, z \mapsto \begin{pmatrix} \mathrm{Re}(z) & \mathrm{Im}(z) \\ -\mathrm{Im}(z) & \mathrm{Re}(z)\end{pmatrix}.$$

And we also use the projection map

$$\pi_{\mathrm{Re}} : M_{2\times 2} \to M_{1\times 2}\,, \begin{pmatrix} a & b \\ c & d\end{pmatrix} \mapsto \begin{pmatrix} a & b\end{pmatrix}.$$

It is easy to check that

$$[\pi_{\mathrm{Re}} \circ \iota(\bar{z})]\,(\iota_0(w)) = \langle \iota_0(z), \iota_0(w)\rangle_{\mathbb{R}^2} = \mathrm{Re}(\bar{z}w)\,. \tag{7.3}$$

Before we go on to study the stability of the reconstruction problem, we provide a clear concept and define the condition number of T subjected to the constraint

$Cx = 0$, denoted as $\kappa(T, \ker(C))$, where $C : \mathbb{R}^P \to \mathbb{R}^Q$ for $Q \leq P$ is another linear operator. First, for the sake of exposition, we denote $C^\perp$ as the set of all matrices E such that its column vectors are linearly independent and span the orthogonal complement of the row space of $C = (C_1, C_2, \ldots, C_n)^T$, i.e.,

$$C^\perp := \{(E_1, E_2, \ldots, E_n) : \langle E_1, \ldots, E_n, C_1, \ldots, C_n\rangle = \mathbb{R}^P, \\ \langle E_1, \ldots, E_{j-1}, E_{j+1}, \ldots, E_n, C_1, \ldots, C_n\rangle \neq \mathbb{R}^P \ \ \forall j\}\,.$$

Now, if we solve the following constraint problem for a given triple (T, b, C),

$$\text{Find } x \in \mathbb{R}^P \text{ such that} \quad Tx = b \quad \text{and} \quad Cx = 0\,,$$

or its least-squares formulation,

$$\min_{\substack{x\in\mathbb{R}^P \\ s.t.\ Cx=0}} ||Tx - b||_2^2\,,$$

we are actually parameterizing the kernel $\ker(C)$ by an orthogonal complement of the row space of C and then solve the equation $Tx = b$ under this parameterization (either in the strict sense or the least-squares sense), i.e., solve for y the equation (with $E \in C^\perp$)

$$(T \circ E)\, y = b$$

or the least-squares minimization (with $E \in C^\perp$)

$$\min_{y\in\mathbb{R}^Q} ||(T \circ E)\, y - b||_2^2\,.$$

From this definition, one can easily get that the operator T is invertible with its solution in the subspace $Cx = 0$ if and only if $T \circ E$ is invertible. One can also directly get that if $Tx = b$ and $T\tilde{x} = \tilde{b}$, where $x, \tilde{x} \in \ker(C)$, then we have the following estimate:

$$\frac{||y - \tilde{y}||}{||y||} \leq \kappa(T \circ E)\frac{||b - \tilde{b}||}{||b||}$$

for any $E \in C^\perp$, where $y, \tilde{y}$ are defined such that $Ey = x, E\tilde{y} = \tilde{x}$. Hence, in order to study the stability of the inversion process of T in the subspace, we are motivated to define the condition number of T under the constraint $Cx = 0$ as

$$\kappa(T, \ker(C)) := \inf\{\kappa(T \circ E) \ : \ E \in C^\perp\}\,. \tag{7.4}$$

7.1.1. A measurement strategy for phaseless reconstruction. In this subsection, we proceed to develop a good measurement strategy which can minimize the condition number of operator T and ensure the well-posedness of the inversion concerned.

Indeed, we shall intuitively expect to have a good strategy in choosing the measurement set $(\theta, \widetilde{\theta}, k)$ by gazing at the vector S_R in (3.6): for a given target resolution N, one may choose $2k_iR\sin((\widetilde{\theta}_i - \theta_i)/2)$ such that they attain the m_0th local extremum of $\mathcal{J}_l$ for $1 < l < N$, i.e., the values of b_{l,m_0} where $\mathcal{J}_l'(b_{l,m_0}) = 0$ for a given m_0. With this particular choice of M sets of measurement data $\{(\theta_i, \widetilde{\theta}_i, k_i)\}_{i=1}^M$ such that $2k_iR\sin((\widetilde{\theta}_i - \theta_i)/2) \in \{b_{1,m_0}, b_{2,m_0}, \ldots, b_{N,m_0}\}$, the operator T is expected to

be well-conditioned and therefore provide a good set of information for the geometry of the inclusion. This shall indeed be verified in this subsection.

In what follows, we aim to estimate, for a given resolution N, the infimum over the condition numbers of all the operators $T : \mathbb{R}^{4N} \to \mathbb{R}^M$ subjected to the constraint $Cx = 0$, i.e.,

$$\kappa_{\inf,N} := \inf\left\{\kappa(T, \ker(C)) \,:\, \{(\theta_i, \widetilde{\theta}_i, k_i)\}_{i=1}^M \in [0.2\pi]^2 \times (0,\infty)\,,\, M \in \mathbb{Z}\right\},$$

by appropriately choosing the vectors $\{(\theta_i, \widetilde{\theta}_i, k_i)\}_{i=1}^M$. Indeed, from the following well-known asymptotic of $\mathcal{J}_l$ [1] for all l,

$$\mathcal{J}_l(z) = \sqrt{\frac{2}{\pi z}}\cos\left(z - \frac{2l+1}{4}\pi\right) + O(z^{-3/2})\,, \tag{7.5}$$

we directly have for a fixed l that

$$b_{l,m_0}\Big/\frac{(4m_0 + 2l + 1)\pi}{4} \to 1 \tag{7.6}$$

as m_0 goes to infinity. Therefore, for a given large m_0, if we choose $(\theta_i, \widetilde{\theta}_i, k_i)$ as the form $(\theta_i, \theta_i + \pi, \frac{4m_0+2J_i+1}{8R})$, where $(J_i)_{i=1}^M \in \mathbb{Z}$ are some integral indices to be specified later, then we have directly from (7.5) and (7.6) that

$$S_R(\theta_i, \widetilde{\theta}_i, k_i)_l = e^{il\theta_i}\sqrt{\frac{16R}{\pi(4m_0 + 2J_i + 1)}}\cos\left(\left(m_0 + \frac{J_i - l}{2}\right)\pi\right) + O(m_0^{-3/2})\,. \tag{7.7}$$

Let T_{m_0} be the linear operator T with this specific arrangement of measurements for a given m_0. If we further denote $L := T_{m_0}^T T_{m_0}$ in the form of a block matrix $(L_{lm})_{-N\le l,m\le N,\, l,m\neq 0}$, then from (7.3) each of the blocks L_{lm} will be the following 2×2 matrix:

$$\begin{aligned} L_{lm} &= \iota_0\left[S_R(\theta_i, \widetilde{\theta}_i, k_i)_l\right]^T \iota_0\left[S_R(\theta_i, \widetilde{\theta}_i, k_i)_m\right] \\ &= \frac{16R}{\pi}\,\iota\left[\sum_{i=1}^M L_{l,m,\theta_i}\frac{1}{4m_0 + 2J_i + 1}\cos\left(\left(m_0 + \frac{J_i - m}{2}\right)\pi\right)\cos\left(\left(m_0 + \frac{J_i - l}{2}\right)\pi\right)\right] + O(m_0^{-2})\,, \end{aligned}$$

where ι_0 and ι are defined as in the beginning of section 7.1, and the matrix $L_{l,m,\theta}$ has the form

$$L_{l,m,\theta} = \begin{pmatrix} \cos(m\theta)\cos(l\theta) & \cos(m\theta)\sin(l\theta) \\ \cos(m\theta)\sin(l\theta) & \sin(m\theta)\sin(l\theta)\end{pmatrix}.$$

For the sake of exposition, we further denote $\theta_i = 2\pi I_i/N$, where $(I_i)_{i=1}^M \in \mathbb{Z}$ are some indices to be chosen later.

We are now ready to specify our choice of indices $\{(I_i, J_i)\}_{i=1}^M$. In particular, we let the array $\{(I_i, J_i)\}_{i=1}^M$ be such that it enumerates the index set $\{(I, J) : 1 \le I \le N, 1 \le J \le N\}$, i.e., we have $M = N^2$. With the above definition, we readily see that

$$\begin{aligned} &L_{lm} \\ &= \frac{16R}{\pi}\sum_{J=1}^N\left[\sum_{I=1}^N L_{l,m,\frac{2\pi I}{N}}\right]\frac{1}{4m_0 + 2J + 1}\cos\left(\left(m_0 + \frac{J - m}{2}\right)\pi\right)\cos\left(\left(m_0 + \frac{J - l}{2}\right)\pi\right) + O(m_0^{-2}) \\ &= \frac{16RN}{\pi}\delta_{|l|,|m|}\begin{pmatrix}1 & 0 \\ 0 & \operatorname{sgn}(l)\operatorname{sgn}(m)\end{pmatrix}\sum_{J=1}^N\frac{1}{4m_0 + 2J + 1}\cos^2\left(\frac{(J-m)\pi}{2}\right) + O(m_0^{-2})\,, \end{aligned}$$

where $\delta_{a,b}$ is the Kronecker delta for any $a, b \in \mathbb{N}$.

From the above summation, we can directly infer that

$$L_{lm} = \frac{16RN}{\pi}\delta_{|l|,|m|}\begin{pmatrix}1 & 0\\ 0 & \operatorname{sgn}(l)\operatorname{sgn}(m)\end{pmatrix}\sum_{J=0}^{[\frac{N-1}{2}]}\frac{1}{4m_0+4J+2\,\mathtt{mod}_2(m)+1}+O(m_0^{-2})\,, \tag{7.8}$$

where $\mathtt{mod}_2$ is the standard mod-2 function and $[\cdot]$ is the floor function. Now, for the sake of exposition, we denote for given $\widetilde{C}, m_0, \widetilde{M}$ a coefficient $K_{\widetilde{C},m_0,\widetilde{M}}$ as

$$K_{\widetilde{C},m_0,\widetilde{M}} := \sum_{J=1}^{\widetilde{M}}\frac{1}{4m_0+1+4J+2\widetilde{C}}\,. \tag{7.9}$$

With this definition, we now hope to approximate $K_{\tilde{C},m_0,\widetilde{M}}$. In fact, from the comparison test, we directly arrive at, for any fixed $m_0, \tilde{M}$ and any $\widetilde{C} = 0, 1$, that the following holds:

$$\frac{1}{4}\log\left(1+\frac{\tilde{M}}{m_0+2}\right) \le K_{C,m_0,\tilde{M}} \le \frac{1}{4}\log\left(1+\frac{\tilde{M}}{m_0+1}\right)\,. \tag{7.10}$$

Then we can write

$$L_{lm} = \frac{16RN}{\pi}\delta_{|l|,|m|}K_{\mathtt{mod}_2(m),m_0,[\frac{N-1}{2}]}\begin{pmatrix}1 & 0\\ 0 & \operatorname{sgn}(l)\operatorname{sgn}(m)\end{pmatrix}+O(m_0^{-2})\,, \tag{7.11}$$

with $K_{\mathtt{mod}_2(m),m_0,[\frac{N-1}{2}]}$ satisfying estimate (7.10). We may now observe a seemingly pathological situation: the matrix L is actually not invertible in $\mathbb{R}^{4N}$. However, this is actually not as pathological as we think it is, because the constraint $Cx = 0$ comes in to play a fundamental role. To proceed, we can take a matrix $E \in C^{\perp}$ in the block form $(E_{lm})_{-N\le l\le N, l\neq 0, 1\le m\le N,}$ as follows:

$$E_{lm} = \delta_{|l|,m}\begin{pmatrix}1 & 0\\ 0 & \operatorname{sgn}(l)\end{pmatrix}\,. \tag{7.12}$$

One can easily check that the above block matrix E is indeed in $C^{\perp}$. Then one can directly calculate that, for all $1 \le l, m \le N$,

$$\left(E^T \circ L \circ E\right)_{lm} = \frac{64RN}{\pi}\delta_{l,m}K_{\mathtt{mod}_2(m),m_0,[\frac{N-1}{2}]}\begin{pmatrix}1 & 0\\ 0 & 1\end{pmatrix}+O(m_0^{-2})\,, \tag{7.13}$$

which is now invertible. Hence for a fixed N and the choice $(\theta_i, \widetilde{\theta}_i, k_i)$ of the form $(2\pi I_i/N, 2\pi I_i/N+\pi, \frac{4m_0+2J_i+1}{8R})$, where $\{(I_i, J_i)\}_{i=1}^{M}$ enumerates through $\{(I, J) : 1 \le I \le N, 1 \le J \le N\}$, we can directly derive the following estimate for the singular values of T_{m_0}:

$$\begin{aligned}\frac{4\sqrt{RN}}{\sqrt{\pi}}\sqrt{\log\left(1+\frac{[\frac{N-1}{2}]}{m_0+2}\right)}-\frac{\tilde{C}_N}{m_0^2} &\le s_{\min}(T_{m_0}\circ E) \le s_{\max}(T_{m_0}\circ E)\\ &\le \frac{4\sqrt{RN}}{\sqrt{\pi}}\sqrt{\log\left(1+\frac{[\frac{N-1}{2}]}{m_0+1}\right)}+\frac{\tilde{C}_N}{m_0^2},\end{aligned}$$

where $\tilde{C}_N$ is a constant only depending on N. Therefore, if we write s_{max} and s_{min}, respectively, as the largest and smallest singular values, then it follows that

$$\begin{aligned}\kappa(T_{m_0}\circ E) &= \frac{s_{\max}(T_{m_0}\circ E)}{s_{\min}(T_{m_0}\circ E)}\\ &\le \sqrt{\log\left(1+\frac{[\frac{N-1}{2}]}{m_0+1}\right)\Big/\log\left(1+\frac{[\frac{N-1}{2}]}{m_0+2}\right)}+O({m_0}^{-2}).\end{aligned}\tag{7.14}$$

The Taylor series of $\log(1+x)$ and $\sqrt{a+x}$ then give rise to the following estimate for large m_0:

$$\begin{aligned}\kappa_{\inf,N} &\le \kappa(T_{m_0},\ker(C)) \le \kappa(T_{m_0}\circ E)\\ &\le \sqrt{\frac{m_0+2}{m_0+1}}+O(m_0^{-2}) \le 1+O(m_0^{-1}),\end{aligned}\tag{7.15}$$

where we should remind ourselves that the big-O terms are bounded by a constant only depending on N. Since m_0 is arbitrary, we get for any given N that the infimum of the condition number $\kappa(T,\ker(C))$ is given by $\kappa_{\inf,N}=1$, and a minimizing sequence to attain this infimum can be actualized by measurements $(\theta_i,\widetilde{\theta}_i,k_i)$ as previously specified as m_0 goes to infinity. This implies that we can always make an appropriate choice of the target resolution N such that the inversion process of T is well-posed. The above analysis can be summarized into the following theorem.

THEOREM 7.1. *For a given target resolution N, the infimum $\kappa_{inf,N}$ of the condition number $\kappa(T,\ker(C))$ defined as in* (7.5) *over the set of linear operators T is given by*

$$\kappa_{inf,N}=1.\tag{7.16}$$

A minimizing sequence $\kappa(T_{m_0},\ker(C))$, $m_0\in\mathbb{Z}$, of this infimum acquires the following bound:

$$\kappa(T_{m_0},\ker(C))\le 1+O(m_0^{-1})\tag{7.17}$$

if we make the arrangement of phaseless measurements in the way that the following equality holds:

$$(\theta_i,\widetilde{\theta}_i,k_i)=\left(2\pi I_i/N,\,2\pi I_i/N+\pi,\,\frac{4m_0+2J_i+1}{8R}\right),\tag{7.18}$$

where $\{(I_i,J_i)\}_{i=1}^{M}$ enumerates through $\{(I,J):1\le I\le N,1\le J\le N\}$ and m_0 is large; hence N^2 phaseless measurements shall be made.

This theorem gives us a very effective strategy of data measurement such that the phaseless reconstruction process shall be well-posed. In particular, an increase of m_0 in the aforementioned measurement method reduces the condition number of the inversion process with an order of $O(m_0^{-1})$ according to (7.17).

7.2. Estimation of the condition number of L. From the previous analysis, we can see that the inversion process of operator T can be made impressively stable and one can suppress its condition number appropriately. However, this does not ensure a very stable phaseless inversion process, owing to the fact from (7.1) that the total inversion process is given by $T^{-1}\circ L^{-1}$.

Although the action of L is simple and explicit, the inversion process may not be as simple as one might think. The condition number of L can be directly calculated as $\max_i |P_R(\theta_i, \widetilde{\theta}_i, k_i)|/\min_i |P_R(\theta_i, \widetilde{\theta}_i, k_i)|$. Therefore the inversion process becomes severely ill-posed when some measurement data has a very small value $|P_R(\theta_i, \widetilde{\theta}_i, k_i)|$, which in turn pushes up the condition number to an arbitrary magnitude. This causes the reconstruction process to be very unstable in practice.

However, a very simple regularization technique can get rid of this instability. Thanks to the fact that $P_R(\theta, \widetilde{\theta}, k)$ is analytic, its value cannot be zero on an open neighborhood, and therefore a simple regularization can be performed on the inversion of L by the operator L_α^{-1} defined as follows:

$$L_\alpha^{-1} = \operatorname{diag}\Bigg(\chi_{x>\alpha}(|P_R(\theta_i, \widetilde{\theta}_i, k_i)|)[P_R(\theta_i, \widetilde{\theta}_i, k_i)]^{-1} + \alpha^{-1}\chi_{x\le\alpha}(|P_R(\theta_i, \widetilde{\theta}_i, k_i)|) \lim_{(\theta,\widetilde{\theta},k)\to(\theta_i,\widetilde{\theta}_i,k_i)} \frac{P_R(\theta, \widetilde{\theta}, k)}{|P_R(\theta, \widetilde{\theta}, k)|} \Bigg), \tag{7.19}$$

where $\chi_{x>\alpha}$ and $\chi_{x\le\alpha}$ are the respective characteristic functions on the intervals $\{x > \alpha\}$ and $\{x \le \alpha\}$. With this definition, we come readily to the following simple but important lemma.

LEMMA 7.2. *Let L_α^{-1} be defined as in* (7.19)*; then we have*

$$\kappa(L^{-1}) = \frac{\max_i |P_R(\theta_i, \widetilde{\theta}_i, k_i)|}{\min_i |P_R(\theta_i, \widetilde{\theta}_i, k_i)|}, \quad \kappa(L_\alpha^{-1}) \le \frac{2}{\alpha}. \tag{7.20}$$

We can see from above that $\kappa(L^{-1})$ cannot be controlled but $\kappa(L_\alpha^{-1})$ has an upper bound; therefore, it provides a stable inversion process if α is appropriately chosen.

From (7.1), a stable shape reconstruction process is therefore provided by $T^{-1} \circ L_\alpha^{-1}$. Indeed, the stability estimates (7.17) and (7.20) for the condition numbers of T^{-1} and L_α^{-1} subjected to $Cx = 0$ ensure the stability of this reconstruction method and provide optimal strategies to lower the degree of ill-posedness for the phaseless reconstruction problem under the corresponding measurement cases. The stability of our proposed method will be verified in the numerical experiments. To the best of our knowledge, these estimates of condition numbers are completely new to the concerned inverse problems in this work.

7.3. A comparison with the phased reconstruction. As we have remarked in section 3, together with the fact that any translation of the inclusion yields the same phaseless measurement, the phaseless reconstruction is not unique in this sense. And the linearized phased and phaseless reconstructions share some fundamental differences. From (3.11) or its Fourier-transformed version (Algorithm 1), we see that any algorithm derived from (3.11) for the phased reconstruction is equivalent to solving $\delta\left(\mathfrak{F}[h]^{est}(l)\right)_{l=-N}^{N} \in \mathbb{C}^{2N} \oplus \{0\} \cong \mathbb{R}^{4N}$ such that

$$\tilde{T}\left[(\delta\,\mathfrak{F}[h])^{est}\right] = G(A_\infty^{\text{meas}}(\theta_i, \widetilde{\theta}_i, k_i)), \tag{7.21}$$

where N satisfies

$$C_0^2 \frac{N^{4N}}{R^{2+4N}} < (\text{SNR})^{1+\alpha/2}$$

for some α, where C_0 is the constant as in Theorem 4.1, and $(\mathfrak{F}[h])^{est}$ is again subjected to the constraints

$$\mathrm{Re}(\mathfrak{F}[h])^{est}(-l) - \mathrm{Re}(\mathfrak{F}[h])^{est}(l) = 0\,, \qquad \mathrm{Im}(\mathfrak{F}[h])^{est}(-l) + \mathrm{Im}(\mathfrak{F}[h])^{est}(l) = 0\,,$$

and the operators G and $\tilde{T}$ above are given, respectively, by

1. $G : \mathbb{C}^M \to \mathbb{C}^M$, the componentwise affine map of a vector, i.e., the action $v_i \mapsto \frac{v_i - \pi R^2 \varepsilon^* k^2 P_R(\theta_i, \widetilde{\theta}_i, k_i)}{2\pi R^2 \varepsilon^* k^2}$;
2. $\tilde{T} : \mathbb{C}^{2N} \to \mathbb{C}^M$, the linear operator $v \mapsto \left(\langle\, v\,, S_R(\theta_i, \widetilde{\theta}_i, k_i)\rangle_{l^2(\mathbb{C})}\right)_{i=1}^M$.

A similar stability analysis for the operator $\tilde{T}$ induced by the phased measurements can be performed on that for the operator $\tilde{T}$ corresponding to the phaseless reconstruction as in section 7.1.1. Since most of the steps are similar to the previous analysis for the phaseless reconstruction, we only provide a sketch of the argument. Again we choose $(\theta_i, \widetilde{\theta}_i, k_i)$ of the form $(2\pi I_i/N, 2\pi I_i/N + \pi, \frac{4m_0+2J_i+1}{8R})$, where $\{(I_i, J_i)\}_{i=1}^M \in \mathbb{Z}$ are some integral indices to be specified, and let $\tilde{T}_{m_0}$ be the linear operator $\tilde{T}$ with this specific arrangement of measurement with a given m_0. Denoting $\tilde{L} := \iota[\tilde{T}_{m_0}^*]\iota[\tilde{T}_{m_0}]$, where ι is defined as in the beginning of section 7.1, a similar argument, along with the fact that ι is an algebra homomorphism, shows for $-N \le l, m \le N$ that

$$\tilde{L}_{lm} = \frac{16R}{\pi}\,\iota\left[\sum_{i=1}^M \tilde{L}_{l,m,\theta_i} \frac{1}{4m_0 + 2J_i + 1} \cos\left(\left(m_0 + \frac{J_i - m}{2}\right)\pi\right) \cos\left(\left(m_0 + \frac{J_i - l}{2}\right)\pi\right)\right] + O(m_0^{-2})\,,$$

where each $\tilde{L}_{l,m,\theta_i} := e^{i(l-m)\theta_i}$ is invertible. Again, letting the array $\{(I_i, J_i)\}_{i=1}^M$ enumerate the index set $\{(I, J) : 1 \le I \le N, 1 \le J \le N\}$, i.e., $M = N^2$ complex (phased) measurements, we have

$$\begin{aligned}
&\tilde{L}_{lm} \\
&= \frac{16R}{\pi} \sum_{J=1}^N \iota\left[\sum_{I=1}^N e^{2\pi i(l-m)I/N}\right] \frac{\cos\left(\left(m_0 + \frac{J-m}{2}\right)\pi\right) \cos\left(\left(m_0 + \frac{J-l}{2}\right)\pi\right)}{4m_0 + 2J + 1} + O(m_0^{-2}) \\
&= \frac{16RN}{\pi}\delta_{l,m} \begin{pmatrix} 1 & 0 \\ 0 & 1 \end{pmatrix} \sum_{J=1}^N \frac{\cos^2\left(\frac{(J-m)\pi}{2}\right)}{4m_0 + 2J + 1} + O(m_0^{-2})\,.
\end{aligned}$$

From here onward, the analysis is the same as in section 7.1.1 to get the same block matrix E such that for all $1 \le l, m \le N$,

$$\left(E^T \circ \tilde{L} \circ E\right)_{lm} = \frac{32RN}{\pi}\delta_{l,m} K_{\mathtt{mod}_2(m), m_0, [\frac{N-1}{2}]} \begin{pmatrix} 1 & 0 \\ 0 & 1 \end{pmatrix} + O(m_0^{-2})\,. \tag{7.22}$$

Now an argument similar to that in section 7.1.1 is applied to get an identical result for the phased reconstruction:

$$\kappa(\tilde{T}_{m_0}, \ker(C)) \le \sqrt{\frac{m_0 + 2}{m_0 + 1}} + O(m_0^{-2}) \le 1 + O(m_0^{-1})\,, \tag{7.23}$$

and by tracing all the constants, we can see the constants represented by big-O's are of the same magnitude as in the phaseless reconstruction. Therefore the ill-posedness in inverting T and $\tilde{T}$ is actually of the same order of magnitude using the same set of measurement angles, and the following result holds.

THEOREM 7.3. *For a given target resolution N, condition number $\kappa(\tilde{T}_{m_0}, \ker(C))$ of the operator $\tilde{T}_{m_0}$ for $m_0 \in \mathbb{Z}$ can be controlled by*

$$\kappa(\tilde{T}_{m_0}, \ker(C)) \leq 1 + O(m_0^{-1}) \tag{7.24}$$

if we make an N^2 complex (phased) measurement arrangement:

$$(\theta_i, \widetilde{\theta}_i, k_i) = \left(2\pi I_i/N, 2\pi I_i/N + \pi, \frac{4m_0 + 2J_i + 1}{8R}\right), \tag{7.25}$$

where $\{(I_i, J_i)\}_{i=1}^M$ enumerates through $\{(I, J) : 1 \leq I \leq N, 1 \leq J \leq N\}$.

Nonetheless, we notice a fundamental difference here between the phased and phaseless reconstructions. For the phased reconstruction, the matrix $\tilde{L}$ is itself invertible; therefore the constraint $Cx = 0$ is redundant. However, in the phaseless reconstruction, this set of constraints is necessary for us to get to a solution in the inversion process. Therefore, to fully exploit the constraints $Cx = 0$, it shall be possible to obtain the same stability estimate for $\tilde{T}$ even if the number of equations represented by the matrix are cut off by half. There are different ways to realize this, and we suggest one of them below. We shall not repeat all the details in the argument again but give only a sketch.

Suppose we choose the set of measurement points $(\theta_i, \widetilde{\theta}_i, k_i)$ to be $\left(2\pi I_i/N, 2\pi I_i/N + \pi, \frac{4m_0+2J_i+1}{8R}\right)$, where $\{(I_i, J_i)\}_{i=1}^M$ enumerates the index set $\{(I, J) : 1 \leq I \leq N/2, 1 \leq J \leq N\}$, but we only measure the real part of the far-field pattern $A_\infty^{\text{meas}}(\theta_i, \widetilde{\theta}_i, k_i)$. Clearly, we have N^2 real (phased) measurements. From the fact that $P_R(\theta_i, \widetilde{\theta}_i, k_i)$ is real, we have

$$\text{Re}\left(\tilde{T}\left[(\delta\,\mathfrak{F}[h])^{est}\right]\right) = \text{Re}\left(G(A_\infty^{\text{meas}}(\theta_i, \widetilde{\theta}_i, k_i))\right) = G\left(\text{Re}(A_\infty^{\text{meas}}(\theta_i, \widetilde{\theta}_i, k_i))\right), \tag{7.26}$$

where G is defined below (7.21). Therefore, by taking only N^2 real (phased) measurements, we are actually dropping half of the equations representing measurements from the imaginary part. Now, in order to distinguish from the previous measurement setting, we denote the operator with these new measurement events as $\tilde{\tilde{T}}_{m_0}$ for a given m_0.

With this very particular choice of real (phased) measurements, we know from (7.3) that the matrix $\tilde{\tilde{T}}_{m_0}$ is coincidentally the same as T_{m_0}. Hence, if we write $\tilde{\tilde{L}} := \tilde{\tilde{T}}_{m_0}^T \tilde{\tilde{T}}_{m_0}$, then $\tilde{\tilde{L}} = L$. Therefore, with the same E as previously chosen, the same argument applies for us to get for all $1 \leq l, m \leq N$ that

$$\left(E^T \circ \tilde{\tilde{L}} \circ E\right)_{lm} = \frac{64RN}{\pi}\delta_{l,m}K_{\texttt{mod}_2(m),m_0,[\frac{N-1}{2}]} + O(m_0^{-2})\,. \tag{7.27}$$

This gives the following result.

THEOREM 7.4. *An effective choice of only N^2 real phased measurement ensures the following bound for the condition number:*

$$\kappa(\tilde{\tilde{T}}_{m_0}, \ker(C)) \leq 1 + O(m_0^{-1})\,. \tag{7.28}$$

Other ways to fully exploit the constraints $Cx = 0$ by dropping at most half of the equations represented by $\tilde{T}$, such as measuring the projection of complex numbers by another phase angle other than taking the real part, or taking only a special set

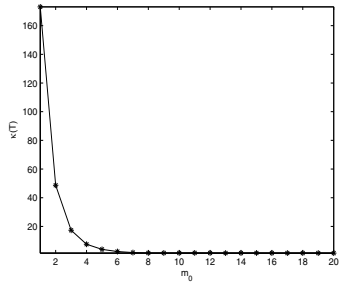

FIG. 1. *Decay of* $\kappa(T, \ker(C))$ *with respect to* m_0.

of undersampling measurements, should be possible, but for the sake of simplicity, we shall not proceed further.

From the above analysis, we can see that although the structures of T and $\tilde{T}$ are fundamentally different, they have similar behavior on their condition numbers. Yet the phaseless reconstruction is still much more ill-posed than the phased counterpart, owing to the following very simple yet important point. In the phaseless reconstruction, we also need to invert L by a regularized inversion process L_α^{-1}; however, in a phased reconstruction, such an inversion of L is unnecessary. Therefore, instability imposed by L exists only in the phaseless reconstruction. Considering this fact, the total regularized inversion of the phaseless reconstruction is still much more ill-posed than the phased counterpart, having its condition number being $1/\alpha$ times that of the phased reconstruction.

8. Numerical experiments. In this section, we will first present numerical results illustrating some behaviors of the condition number $\kappa(T_{m_0}, \ker(C))$ using our measurement strategy described in section 7.1 and then focus on the inverse problem of shape reconstruction from the observed magnitude of far-field data.

8.1. Condition number of T subjected to $Cx = 0$. In what follows, we observe the behaviors of the condition number $\kappa(T_{m_0}, \ker(C))$ using our measurement strategy given in Theorem 7.3 and check the asymptotic estimate of $\kappa(T)$ in the theorem as m_0 grows. With a given m_0, we now fix the resolution $N = 51$ and choose the wave-numbers k such that $k = \frac{4m_0+2J+1}{8R}$ with $R = 0.2$ and $J = 5, \ldots, 10$. The measurement points are the same as stated in Theorem 7.3. We compute the condition number of the operator T with $m_0 = 1, \ldots, 20$. The values of the corresponding condition numbers are plotted in Figure 1.

We see clearly the drastic decay of the condition number as m_0 grows, showing the effectiveness of increasing stability by the increment of m_0. This agrees with the result we obtained in Theorem 7.3.

8.2. Phaseless reconstruction. We shall now proceed to present several numerical examples to show the performance of the newly proposed reconstruction algorithm, i.e., Algorithm 2 in section 6.1, from phaseless far-field data. In order to attain the robustness and stability of our algorithm, we approximate the inversion of L in step 2 by L_α as in section 7.2 for some regularization α described below.

In the following three examples, we consider an infinite homogeneous background medium with its material coefficient being 1. In each example, an inhomogeneous inclusion $D = B^\delta$ is then introduced as a perturbation of a circular domain $B = B_R(0)$

for some $\delta > 0$ and its radius $R = 0.2$ sitting inside the homogeneous background medium, with its contrast always set to be $\varepsilon^* = 0.05$.

Given a domain B^δ, we first obtain the observed data of the forward problem, namely the magnitude of far-field data. In order to generate the far-field data for the forward problem and the observed scattering coefficients, we use the SIES-master package developed by Wang [54]. For a fixed wave-number k, we first solve for the solutions (ϕ_m, ψ_m) of (2.8) for $|m| \leq 50$ using the rectangular quadrature rule with mesh-size $s/1024$ along the boundary of the target, where s denotes the length of the inclusion boundary. The scattering coefficients of B^δ of orders (n, m) for $|n|, |m| \leq 50$ are then calculated, and the far-field data $A(\theta_d, \theta_x, k)$ is evaluated using (2.10) with $\theta_d, \theta_x \in (0, 2\pi]$ on a uniform mesh of size $N = 50$. Then the magnitude of the far-field pattern $|A(\theta_d, \theta_x, k)|$ is taken for our reconstruction process. In order to test the robustness of our reconstruction algorithm against the noise, we introduce some multiplicative random noise in the magnitude of far-field pattern $|A(\theta_d, \theta_x, k)|$ pointwisely in the form

$$|A^{\text{meas}}(\theta_d, \theta_x, k)|^\sigma = |A^{\text{meas}}(\theta_d, \theta_x, k)|(1 + \sigma\,\xi), \tag{8.1}$$

where ξ is uniformly distributed between $[-1, 1]$ and σ refers to the relative noise level. In the following four examples, we always set the noise level to be $\sigma = 5\%$.

Then we apply our reconstruction algorithm for shape reconstruction with the noisy phaseless data as $T^{-1} \circ L_\alpha^{-1} \circ F$ following the notation introduced in section 7, where the regularization parameter is chosen as $\alpha = 10^{-3}$. In view of (7.18), we make the choice of measurements such that the measured wave-numbers k satisfy $k = \frac{4m_0+2J+1}{8R}$ with $m_0 = 10$ in all the examples, and $J = 5, \ldots, 5 + \tilde{C}$ for some $\tilde{C}$ to be chosen in each of the examples. The relative error of the reconstruction is defined by

$$\text{Relative Error} := \frac{\text{Area}\,((D^{\text{approx}} \bigcup D) \backslash (D^{\text{approx}} \bigcap D))}{\text{Area}(D)}\,, \tag{8.2}$$

where D^{approx} is the reconstructed domain of the exact one D. To demonstrate the effectiveness of our algorithm and illustrate the necessity of a certain number of measurements angles in the phaseless reconstruction (i.e., to test its resolution limit), we try three different sets of measurements angles:

Set 1 Full measurement angles (overabundant number of measurements):

$$((\theta_d)_i, (\theta_x)_i) = (2\pi I_i/N_0, 2\pi K_i/N_0)\,, \quad 1 \leq I_i, K_i \leq N_0\,, \tag{8.3}$$

where N_0 is always chosen as 50 in all the examples.

Set 2 Transmission measurement angles (critical number of measurements):

$$((\theta_d)_i, (\theta_x)_i) = (2\pi I_i/N, 2\pi I_i/N + \pi + U)\,, \quad 1 \leq I_i \leq N\,, \tag{8.4}$$

where $N := \min\{N : [\mathfrak{F}(h)](k) = 0\,, |k| > N\}$ and h is the perturbation in the corresponding example and $U = (-\frac{\pi}{5}, \frac{\pi}{5})$. In particular, transmission data refers to the measurement of $A(\theta_d, \theta_x, k)$ where $\theta_d = \theta_x + \pi$.

Set 3 Half of transmission measurement angles (insufficient number of measurements):

$$\begin{aligned} &((\theta_d)_i, (\theta_x)_i) = (2\pi I_i/[[N/2]], 2\pi I_i/[[N/2]] + \pi + U)\,, \\ &1 \leq I_i \leq [[N/2]]\,, \end{aligned} \tag{8.5}$$

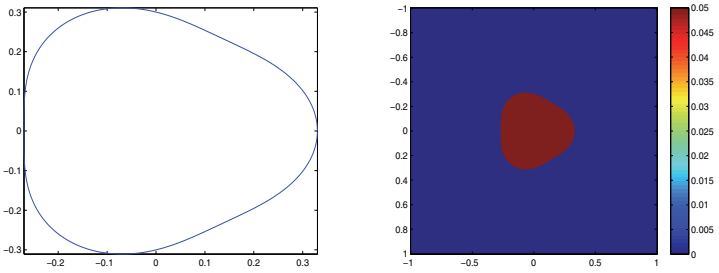

FIG. 2. *Exact inhomogeneous domain (left) and the contrast of the inclusion (right) in Example* 1.

which consists of $[[N/2]]$ measurement angles, where N is the same as previously mentioned and $[[\cdot]]$ is the ceiling function.

The purpose of introducing an interval U instead of one single point is to increase numerical stability in reconstruction. We emphasize that **Sets 2** and **3** are set up only to test the resolution limit of our phaseless reconstruction algorithm. We are not suggesting the necessity to determine $\min\{N : [\mathfrak{F}(h)](k) = 0\,, |k| > N\}$ from h before utilizing our algorithm. Such information is unnecessary and unavailable in a practical phaseless reconstruction.

In order to further increase numerical stability using a critical number of measurements (**Set 2**) and an insufficient number of measurement (**Set 3**), we further regularize our inversion process by an L^1 regularizer to enforce sparsity in the Fourier modes of our reconstructed perturbation; i.e., we solve

$$\min_{C\mathbf{X}=0} ||(L_\alpha \circ T)\mathbf{X} - F(|A_\infty^{\text{meas}}(\theta, \widetilde{\theta}, k)|)||_2^2 + \beta||\mathbf{X}||_1, \tag{8.6}$$

where β is a regularization parameter that is always chosen as $\beta = 0.05$. We perform the L^1 minimization by a standard Bregman iteration [49].

Example 1. In this example, we consider an inhomogeneous domain of a floriform shape $D = B^\delta$ described by the following parametric form (with $\delta = 0.1$ and $n = 3$):

$$r = 0.2(1 + \delta\cos(n\theta))\,, \quad \theta \in (0, 2\pi]\,, \tag{8.7}$$

which is a perturbation of the domain $B = B(0, 0.2)$; see Figure 2(left) and (right), respectively, for the shape of the domain and the contrast of the inhomogeneous medium.

The magnitudes of the far-field pattern for six wave-numbers are used for shape reconstruction, i.e., $\tilde{C} = 5$, and the Fourier coefficients of the reconstructed perturbations using the respective measurement sets are shown in Figure 3.

Although there are some deficiencies in the reconstruction of Fourier modes, we can see from these figures that the Fourier coefficients reconstructed from **Set 1** are largest at $|n| = 3$ with its magnitude almost between 0.04 and 0.05, which clearly indicates a strong dominance of $\delta\cos(3\theta)$ with magnitude δ between 0.08 and 0.1 and corresponds to the signal from the exact inclusion. The reconstruction from **Set 2** has more deficiency, being that the Fourier mode is somehow shifted to $\delta(\cos(3\theta)+\sin(3\theta))$ with magnitude δ between 0.02 and 0.025. However, the location of the peak Fourier mode is still correct. Nonetheless, the reconstruction from **Set 3** deviates totally

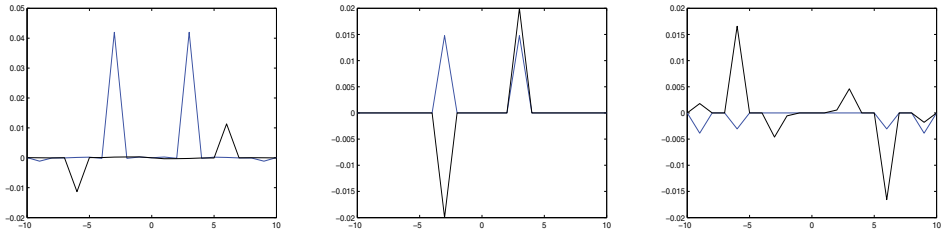

FIG. 3. *Fourier coefficients of reconstructed perturbations in Example* 1*;* ***Sets* 1** *to* ***Set* 3** *from left to right; blue: real part; black: imaginary part. Color is available online only.*

from the exact solution, indicating its insufficiency in number of measurements to reconstruct the perturbation. This goes with the theoretical analysis in section 7.1.1.

Now we show in Figure 4(top) the shapes of reconstructed domains, Figure 4(middle) the contrast of the reconstructed media, and Figure 4(bottom) a comparison between the reconstructed domains D^{approx} and exact domain D using the values of a sum of characteristic functions $\chi_D + \chi_{D^{\text{approx}}}$. The relative L^2 errors of the reconstructions for **Set 1** to **Set 3** are, respectively, 3.29%, 6.34%, and 11.72%. In view of the severe ill-posedness of the phaseless reconstruction problem and 5% percent of measurement noise, the reconstructions from **Set 1** and **Set 2** measurements are quite reasonable

Example 2. We test another domain of the flori-form shape described by (8.7) with $\delta = 0.1$ and $n = 5$. Figure 5(left) and (right) show the shape of the domain and the contrast of the inhomogeneous medium, respectively.

In this example, the magnitudes of the far-field pattern for 16 wave-numbers are used for shape reconstruction, i.e., $\tilde{C} = 15$. The Fourier coefficients of the reconstructed perturbations using the respective measurement sets are shown in Figure 6.

We can now see that both reconstructions from **Set 1** and **Set 2** are reasonable and indicate the correct peak Fourier modes and their magnitudes. It is no surprise to see that the reconstruction for **Set 2** is worse than that for **Set 1**. However, we can see that in this particular case, the reconstruction for **Set 3** coincidentally collides with the exact solution after regularization.

In Figure 7(top), (middle), and (bottom), the shapes of reconstructed domains, the contrast of the reconstructed media, and the comparison between the reconstructed domains D^{approx} and exact domain D (by showing a sum of characteristic functions $\chi_D + \chi_{D^{\text{approx}}}$) are presented, respectively. The relative L^2 errors of the reconstructions for **Set 1** to **Set 3** are, respectively, 4.91%, 6.94%, and 0.57%. As we mentioned above, quite surprisingly, the L^1 regularizer coincidentally provides a very good estimate for **Set 3**.

Example 3. In this last example, we test a domain of more complicated flori-form shape $D = B^\delta$ described by the following parametric form (with $\delta = 0.1$ and $n = 3$):

$$r = 0.2(1 + \delta\cos(n\theta) + 2\delta\cos(2n\theta)), \quad \theta \in (0, 2\pi]. \tag{8.8}$$

The shape of the domain is given in Figure 8(left) and the contrast of the inhomogeneous medium in Figure 8(right).

The magnitudes of the far-field pattern for six wave-numbers are used for shape

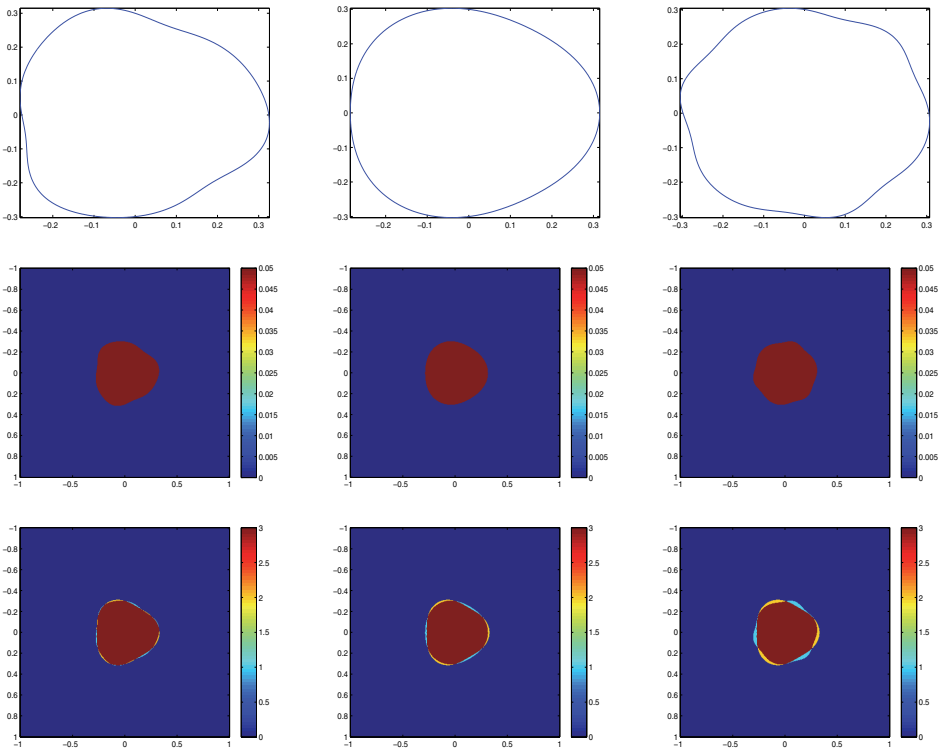

FIG. 4. *Reconstructed domain and medium in Example* 1 *and comparison between the exact and reconstructed domains;* ***Set* 1** *to* ***Set* 3** *from left to right; from top to bottom: reconstructed shape, reconstructed inclusion, and comparison between reconstructed and exact domains.*

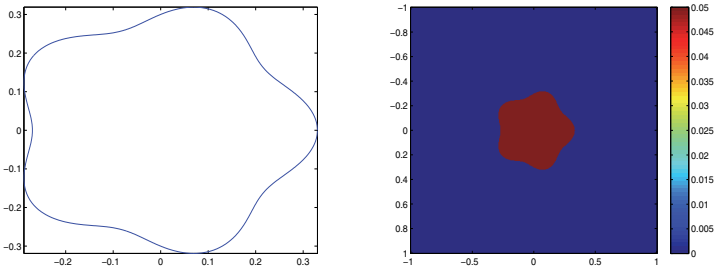

FIG. 5. *Exact inhomogeneous domain (left) and the contrast of the inclusion in Example* 2.

reconstruction, i.e., $\tilde{C} = 5$, and the Fourier coefficients of the reconstructed perturbations using the respective measurement sets are shown in Figure 9.

In this example, as we can see, the reconstruction from **Set 1** is the best, with both the peak Fourier modes and their magnitudes quite close to the exact one, although with some phase shifts. Reconstruction from **Set 2** is still reasonable. The magnitude of the sixth Fourier modes is closer to the exact one; however, that of the third mode deviates further from the exact one, and it has more phase shifts. Reconstruction from **Set 3** is the worst, with great deficiency from the exact perturbation,

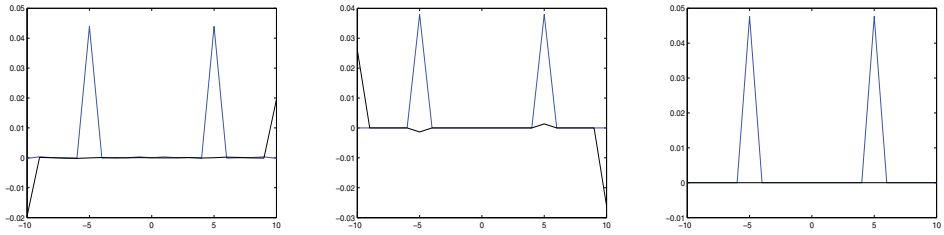

FIG. 6. *Fourier coefficients of reconstructed perturbations in Example* 2*;* ***Set* 1** *to* ***Set* 3** *from left to right; blue: real part; black: imaginary part. Color is available online only.*

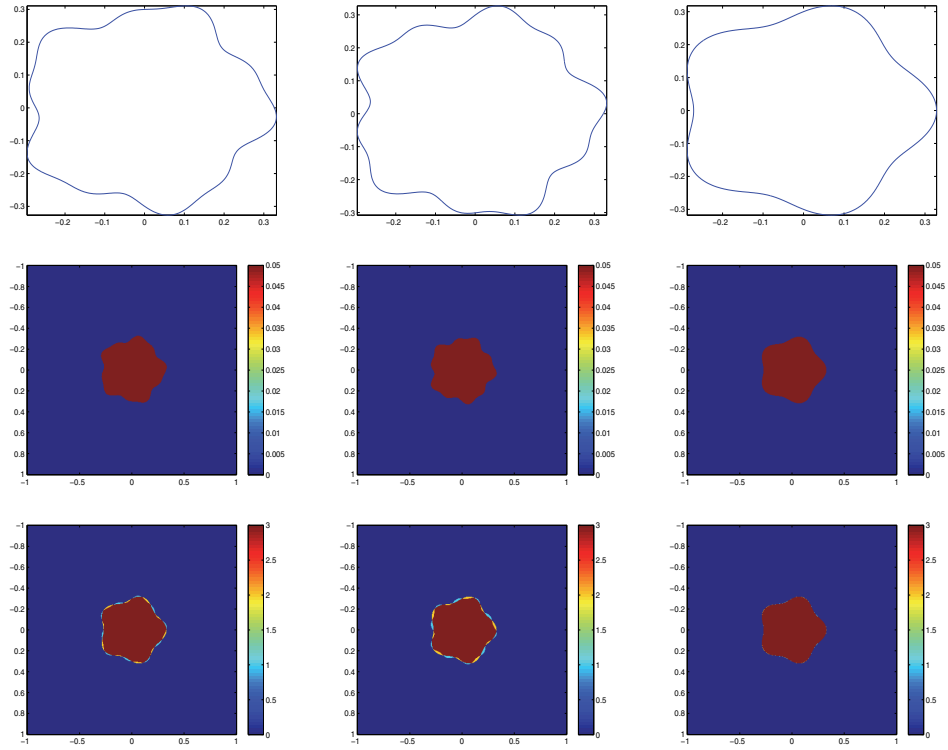

FIG. 7. *Reconstructed domain and medium in Example* 2 *and comparison between the exact and reconstructed domains.* ***Set* 1** *to* ***Set* 3** *from left to right; reconstructed shape, reconstructed inclusion, and comparison between reconstructed and exact domains from top to bottom.*

considering the fact this reconstruction gives us many modes that do not exist in the exact perturbation.

In Figure 10(top), (middle), and (bottom), the shapes of reconstructed domains, the contrast of the reconstructed media, and a comparison between the reconstructed domains D^{approx} and exact domain D are presented, respectively. The relative L^2 errors of the reconstructions for **Set 1** to **Set 3** are, respectively, 11.61%, 13.48%, and 14.84%. This indicates that the reconstruction for **Set 1** is the best, that for

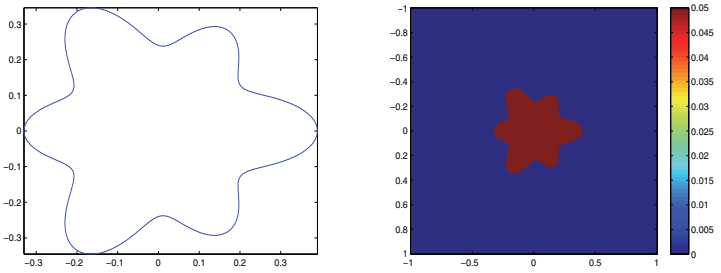

FIG. 8. *Exact inhomogeneous domain (left) and contrast of the inclusion (right) in Example* 3.

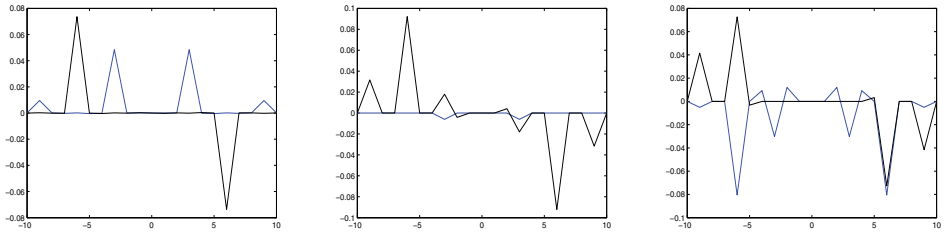

FIG. 9. *Fourier coefficients of reconstructed perturbations in Example* 3*;* ***Set* 1** *to* ***Set* 3** *from left to right; blue: real part; black: imaginary part. Color is available online only.*

Set 2 is still good, and that for **Set 3** is the worst. This goes with the theory we discussed in section 7.1.1.

The reconstructions for **Set 1** (overabundant number of measurements) and **Set 2** (critical number of measurements) are quite reasonable, considering the severe ill-posedness of the phaseless reconstruction problem and a 5% percent measurement noise.

9. Concluding remarks. In this work we have performed sensitivity, resolution, and stability analysis of the phased and phaseless reconstructions using the concept of the scattering coefficients in two dimensions and compared the stability and the degree of ill-posedness of the phased and phaseless reconstructions in terms of the condition numbers of the inversion processes. Our approach can be naturally extended to the three-dimensional case with the help of spherical harmonics to describe the ill-posedness of phased and phaseless reconstructions. As our proposed reconstruction method in this work is based on the evaluation of the Fourier coefficients of the perturbation on a unit circle, it is limited to the reconstructions of star-like shapes. Nonetheless, considering the fact that the definition of scattering coefficients is not restricted to star-shape domains, along with the relationship between geometric motions of the inclusions and algebraic rules of scattering coefficients [6, 8], we anticipate a possible extension of our method to multiply connected domains as well as nonstar like shapes, which will be explored in our future work.

Acknowledgments. The authors would like to thank the two anonymous referees for their many insightful and constructive comments and suggestions, which have led to a great improvement of the results and organization of this work.

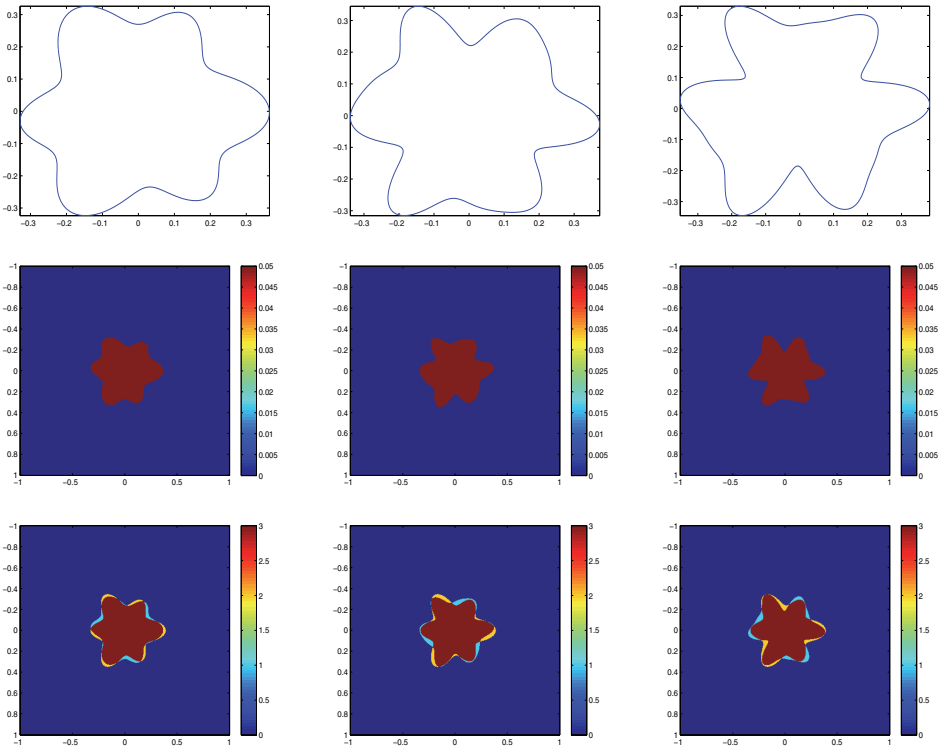

FIG. 10. *Reconstructed domain and medium in Example* 3 *and comparison between the exact and reconstructed domains;* ***Set* 1** *to* ***Set* 3** *from left to right; reconstructed shape, reconstructed inclusion, and comparison between reconstructed and exact domains from top to bottom.*

REFERENCES

[1] M. ABRAMOWITZ AND I. A. STEGUN, *Handbook of Mathematical Functions*, Dover, New York, 1970.

[2] A. ABUBAKAR AND P. M. VAN DEN BERG, *The contrast source inversion method for location and shape reconstructions*, Inverse Problems, 18 (2002), pp. 495–510, http://dx.doi.org/10.1088/0266-5611/18/2/313.

[3] A. ABUBAKAR, P. M. VAN DEN BERG, AND J. T. FOKKEMA, *Time-lapse TM-polarization electromagnetic imaging*, Int. J. Subsurface Sens. Tech. Appl., 4 (2003), pp. 117–135, http://dx.doi.org/10.1023/A:1023067631716.

[4] A. ABUBAKAR, P. M. VAN DEN BERG, AND J. J. MALLORQUI, *Imaging of biomedical data using a multiplicative regularized contrast source inversion method*, IEEE Trans. Microw. Theory Tech., 50 (2002), pp. 1761–1771, http://dx.doi.org/10.1109/TMTT.2002.800427.

[5] H. AMMARI, Y. T. CHOW, AND J. ZOU, *Super-resolution in Imaging High Contrast Targets from the Perspective of Scattering Coefficients*, preprint, 2015.

[6] H. AMMARI, Y. T. CHOW, AND J. ZOU, *The concept of heterogeneous scattering coefficients and its application in inverse medium scattering*, SIAM J. Math. Anal., 46 (2014), pp. 2905–2935, http://dx.doi.org/10.1137/130941468.

[7] H. AMMARI, J. GARNIER, H. KANG, M. LIN, AND S. YU, *Generalized polarization tensors for shape description*, Numer. Math., 126 (2014), pp. 119–224, http://dx.doi.org/10.1007/s00211-013-0561-5.

[8] H. AMMARI, H. KANG, H. LEE, AND M. LIM, *Enhancement of near-cloaking. Part* II: *The Helmholtz equation*, Comm. Math. Phys., 317 (2013), pp. 485–502, http://dx.doi.org/10.1007/s00220-012-1620-y.

[9] H. AMMARI, M. P. TRAN, AND H. WANG, *Shape identification and classification in echolocation*,

SIAM J. Imaging Sci., 7 (2014), pp. 1883–1905, http://dx.doi.org/10.1137/14096164X.

[10] G. Bao and P. Li, *Inverse medium scattering for the Helmholtz equation at fixed frequency*, Inverse Problems, 21 (2005), pp. 1621–1641, http://dx.doi.org/10.1088/0266-5611/21/5/007.

[11] K. Belkebir and M. Saillard, *Special section: Testing inversion algorithms against experimental data*, Inverse Problems, 17 (2001), pp. 1565–1571, http://dx.doi.org/10.1088/0266-5611/17/6/301.

[12] E. J. Candes, X. Li, and M. Soltanolkotabi, *Phase retrieval from coded diffraction patterns*, Appl. Comput. Harmon. Anal., 39 (2015), pp. 277–299, http://www.sciencedirect.com/science/article/pii/S1063520314001201.

[13] E. J. Candes, T. Strohmer, and V. Voroninski, *PhaseLift: Exact and stable signal recovery from magnitude measurements via convex programming*, Comm. Pure Appl. Math., 66 (2013), pp. 1241–1274, http://dx.doi.org/10.1002/cpa.21432.

[14] S. Caorsi, A. Massa, M. Pastorino, and A. Randazzo, *Electromagnetic detection of dielectric scatterers using phaseless synthetic and real data and the memetic algorithm*, IEEE Trans. Geosci. Remote Sens., 41 (2003), pp. 2745–2753, http://dx.doi.org/10.1109/TGRS.2003.815676.

[15] X. Chen, *Application of signal-subspace and optimization methods in reconstructing extended scatterers*, J. Opt. Soc. Amer. A, 26 (2009), pp. 1022–1026, http://dx.doi.org/10.1364/JOSAA.26.001022.

[16] X. Chen, *Subspace-based optimization method for solving inverse-scattering problems*, IEEE Trans. Geosci. Remote Sens., 48 (2010), pp. 42–49, http://dx.doi.org/10.1109/TGRS.2009.2025122.

[17] D. Colton and R. Kress, *Inverse Acoustic and Electromagnetic Scattering Theory*, 2nd ed., Springer-Verlag, Berlin, 1998.

[18] L. Crocco, M. D'Urso, and T. Isernia, *Faithful non-linear imaging from only-amplitude measurements of incident and total fields*, Opt. Express, 15 (2007), pp. 3804–3815, http://dx.doi.org/10.1364/OE.15.003804.

[19] T. J. Cui, Y. Qin, G. L. Wang, and W. C. Chew, *Low-frequency detection of two-dimensional buried objects using high-order extended Born approximations*, Inverse Problems, 20 (2004), pp. S41–S62, http://dx.doi.org/10.1088/0266-5611/20/6/S04.

[20] L. Demanet and P. Hand, *Stable optimizationless recovery from phaseless linear measurements*, J. Fourier Anal. Appl., 20 (2014), pp. 199–221.

[21] M. D'Urso, K. Belkebir, L. Crocco, T. Isernia, and A. Litman, *Phaseless imaging with experimental data: Facts and challenges*, J. Opt. Soc. Amer. A, 25 (2008), pp. 271–281, http://dx.doi.org/10.1364/JOSAA.25.000271.

[22] K. Ito, B. Jin, and J. Zou, *A direct sampling method to an inverse medium scattering problem*, Inverse Problems, 28 (2012), 025003, http://dx.doi.org/10.1088/0266-5611/29/9/095018.

[23] O. Ivanyshyn and R. Kress, *Identification of sound-soft 3D obstacles from phaseless data*, Inverse Probl. Imaging, 4 (2010), pp. 131–149, http://dx.doi.org/10.3934/ipi.2010.4.131.

[24] A. Kirsch, *The MUSIC-algorithm and the factorization method in inverse scattering theory for inhomogeneous media*, Inverse Problems, 18 (2002), pp. 1025–1040, http://dx.doi.org/10.1088/0266-5611/18/4/306.

[25] M. V. Klibanov, *On the first solution of a long standing problem: Uniqueness of the phaseless quantum inverse scattering problem in* 3*-d*, Appl. Math. Lett., 37 (2014), pp. 82–85, http://dx.doi.org/10.1016/j.aml.2014.06.005.

[26] M. V. Klibanov, *Phaseless inverse scattering problems in three dimensions*, SIAM J. Appl. Math., 74 (2014), pp. 392–410, http://dx.doi.org/10.1137/130926250.

[27] M. V. Klibanov, L. H. Nguyen, and K. Pan, *Nanostructures Imaging via Numerical Solution of a* 3*-D Inverse Scattering Problem without the Phase Information*, preprint, arXiv:1510.00659.

[28] M. V. Klibanov and V. G. Romanov, *Explicit formula for the solution of the phaseless inverse scattering problem of imaging of nano structures*, J. Inverse Ill-Posed Probl., 23 (2015), pp. 187–193, http://dx.doi.org/10.1515/jiip-2015-0004.

[29] R. Kress and W. Rundell, *Inverse obstacle scattering with modulus of the far field pattern as data*, in Inverse Problems in Medical Imaging and Nondestructive Testing (Oberwolfach, 1996), Springer, Vienna, 1997, pp. 75–92, http://dx.doi.org/10.1007/978-3-7091-6521-8_7.

[30] J. Li, H. Liu, and J. Zou, *Multilevel linear sampling method for inverse scattering problems*, SIAM J. Sci. Comput., 30 (2008), pp. 1228–1250, http://dx.doi.org/10.1137/060674247.

[31] J. Li, H. Liu, and J. Zou, *Strengthened linear sampling method with a reference ball*, SIAM J. Sci. Comput., 31 (2009), pp. 4013–4040, http://dx.doi.org/10.1137/080734170.

[32] L. L. Li, H. Zheng, and F. Li, *Two-dimensional contrast source inversion method with phase-*

less data: TM case, IEEE Trans. Geosci. Remote Sens., 47 (2009), pp. 1719–1736, http://dx.doi.org/10.1109/TGRS.2008.2006360.

[33] C. W. Liao, M. A. Fiddy, and C. L. Byrne, *Imaging from the zero locations of far-field-intensity data*, J. Opt. Soc. Amer. A, 14 (1997), pp. 3155–3161, http://dx.doi.org/10.1364/JOSAA.14.003155.

[34] A. Litman and K. Belkebir, *Two-dimensional inverse profiling problem using phaseless data*, J. Opt. Soc. Amer. A, 23 (2006), pp. 2737–2746, http://dx.doi.org/10.1364/JOSAA.23.002737.

[35] K. Liu, Y. Xu, and J. Zou, *A parallel radial bisection algorithm for inverse scattering problems*, Inverse Probl. Sci. Eng., 21 (2013), pp. 197–209, http://dx.doi.org/10.1080/17415977.2012.686498.

[36] K. Liu and J. Zou, *A multilevel sampling algorithm for locating inhomogeneous media*, Inverse Problems, 29 (2013), 095003, http://dx.doi.org/10.1088/0266-5611/29/9/095003.

[37] S. Mallat and I. Waldspurger, *Phase retrieval for the Cauchy wavelet transform*, J. Fourier Anal. Appl., 21 (2015), pp. 1251–1309, http://dx.doi.org/10.1007/s00041-015-9403-4.

[38] E. A. Marengo, F. K. Gruber, and F. Simonetti, *Time-reversal MUSIC imaging of extended targets*, IEEE Trans. Image Process., 16 (2007), pp. 1967–1984, http://dx.doi.org/10.1109/TIP.2007.899193.

[39] R. G. Novikov, *Explicit formulas and global uniqueness for phaseless inverse scattering in multidimensions*, J. Geom. Anal., 26 (2016), pp. 346–359, http://dx.doi.org/10.1007/s12220-014-9553-7.

[40] R. G. Novikov, *Formulas for phase recovering from phaseless scattering data at fixed frequency*, Bull. Sci. Math., 139 (2015), pp. 923–936, http://dx.doi.org/10.1016/j.bulsci.2015.04.005.

[41] R. Potthast, *A survey on sampling and probe methods for inverse problems*, Inverse Problems, 22 (2006), pp. R1–R47, http://dx.doi.org/10.1088/0266-5611/22/2/R01.

[42] T. Takenaka, D. Wall, H. Harada, and M. Tanaka, *Reconstruction algorithm of the refractive index of a cylindrical object from the intensity measurements of the total field*, Microw. Opt. Technol. Lett., 14 (1997), pp. 182–188, http://dx.doi.org/10.1002/(SICI)1098-2760(19970220)14:3%3C182::AID-MOP15%3E3.0.CO;2-A.

[43] C. Torresverdin and T. M. Habashy, *Rapid* 2.5*-dimensional forward modeling and inversion via a new nonlinear scattering approximation*, Radio Sci., 29 (1994), pp. 1051–1079, http://dx.doi.org/10.1029/94RS00974.

[44] P. M. van den Berg and A. Abubakar, *Contrast source inversion method: State of art*, Prog. Electromagn. Res. PIER, 34 (2001), pp. 189–218, http://dx.doi.org/10.2528/PIER01061103.

[45] P. M. van den Berg, A. Abubakar, and J. T. Fokkema, *Multiplicative regularization for contrast profile inversion*, Radio Sci., 38 (2003), pp. 23-1–23-10, http://dx.doi.org/10.1029/2001RS002555.

[46] P. M. van den Berg and R. E. Kleinman, *A contrast source inversion method*, Inverse Problems, 13 (1997), pp. 1607–1620, http://dx.doi.org/10.1088/0266-5611/13/6/013.

[47] P. M. van den Berg, A. L. van Broekhoven, and A. Abubakar, *Extended contrast source inversion*, Inverse Problems, 15 (1999), pp. 1325–1344, http://dx.doi.org/10.1088/0266-5611/15/5/315.

[48] G. N. Watson, *A Treatise on the Theory of Bessel Functions*, reprint of 2nd ed., Cambridge University Press, Cambridge, UK, 1966.

[49] W. Yin, S. Osher, D. Goldfarb, and J. Darbon, *Bregman iterative algorithms for* l_1*-minimization with applications to compressed sensing*, SIAM J. Imaging Sci., 1 (2008), pp. 143–168, http://dx.doi.org/10.1137/070703983.

[50] M. S. Zhdanov and S. Fang, *Three-dimensional quasi-linear electromagnetic inversion*, Radio Sci., 31 (1996), pp. 741–754, http://dx.doi.org/10.1029/96RS00719.

[51] M. S. Zhdanov and G. Hursan, 3*D electromagnetic inversion based on quasi-analytical approximation*, Inverse Problems, 16 (2000), pp. 1297–1322, http://dx.doi.org/10.1088/0266-5611/16/5/311.

[52] H. Zheng, L. Li, and F. Li, *A multi-frequency MRCSI algorithm with phaseless data*, Inverse Problems, 25 (2009), pp. 1–13, http://dx.doi.org/10.1088/0266-5611/25/6/065006.

[53] H. Zheng, M.-Z. Wang, Z. Zhao, and L. Li, *A novel linear EM reconstruction algorithm with phaseless data*, Prog. Electromagn. Res. Lett., 14 (2010), pp. 133–146, http://dx.doi.org/10.2528/PIERL10031306.

[54] H. Wang, *Codes on Scattering Coefficients*, unpublished manuscript.